Construction of PCL/SF-based electrospun nanofibers for skin tissue engineering applications

By Gülşah YILDIZ

Submitted to Graduate School of Engineering and Natural Sciences in

partial fulfillment of the requirements for the degree of

Master of Sciences

Sabancı University

July 2023

To my Family

Construction of PCL/SF-based Electrospun Nanofibers for Skin Tissue Engineering Applications

Gülşah Yıldız

Manufacturing Engineering, M.Sc. Thesis, 2023

Thesis Advisor: Prof. Dr. Yusuf Z. Menceloğlu

Keywords: Electrospinning, PCL, Silk Fibroin, polymer nanofibers, biomaterials, skin engineering

ABSTRACT

Skin substitutes hold great potential for the treatment of high-degree burns and chronic wounds. Current solutions, including Integra Dermal Template, provide fast and practical treatments for skin defects. However, existing templates cannot provide a solution for the recreation of the native tissue functionality and scarless healing of the wounded site. This study examines the construction and characterization of novel skin substitutes based on PCL/SF blends. According to the morphological analysis, each sample had a homogenous fiber distribution without any beads. It was shown that the thermal stability of nanofibers improved with the incorporation of SF into the PCL structure. Mechanical analysis proved that the addition of SF into PCL enhanced tensile strength by providing intermolecular interactions due to SF functional groups. In addition, Young's modulus of the samples improved with the addition of some SF since it increases the stiffness and the structural integrity of the fiber structure. Water contact analysis demonstrated that all samples obtained adequate hydrophilicity, other than PCL, which is important to maintain cell functionality. Lastly, cell proliferation and viability assays were performed by seeding the scaffolds with primary human keratinocytes. It was observed that using

blends of PCL/SF led to better cell proliferation and viability compared to pure PCL and SF scaffolds.

Deri Doku Mühendisliği Uygulamaları için Elektroeğirme Yöntemiyle PCL/İF-Temelli Nanofilm Yapıların Oluşturulması

Gülşah Yıldız

Üretim Mühendisliği, Yüksek Lisans Tezi, 2023

Tez Danışmanı: Prof. Dr. Yusuf Z. Menceloğlu

Anahtar Kelimeler: Elektroeğirme, PCL, İpek Fibroin, Polimer nanolifler, biyomalzeme, deri doku mühendisliği

ÖZET

Deri eşdeğerleri yüksek dereceli yanıklar ve kronik yaralarda kullanılmak için iyi bir potansiyel göstermektedirler. Integra deri eşdeğeri benzeri halihazırda kullanılan yöntemler deri bozuklukları için hızlı ve kullanışlı bir çözüm olarak öne çıkmaktadırlar. Fakat kullanılan bu yöntemler derinin kendini yenileyip doğal deri yapısının inşaasında ve yara izsiz iyileşme sağlanmasında yetersiz kalmaktadırlar. Bu çalışmada özgün PCL/İF-temelli bir deri eşdeğerinin üretilmesi ve karakterizasyonunun yapılmasını ele alınmıştır. Morfolojik analizlere göre bütün örnekler homojen bir fiber dağılımı göstermiş olup fiberlerde herhangi bir boncuk yapısına rastlanmamıştır. PCL yapısına İF eklenmesinin fiber termal stabilitesini arttırdığı gösterilmiştir. PCL yapısına eklenen İF' nin fiberler arasında intermoleküler etkileşim sağlayarak fiberlerin mekanik gücünü arttırdığı kanıtlanmıştır. Ayrıca, İF eklenmesi örneklerin bükülmezliğini ve yapısal bütünlüğünü geliştirip Young modüllerini arttırmıştır. Temas açısı testleri PCL hariç bütün örneklerin hücre işlevselliğini sürdürmesi için yeterli hidrofilisiteye sahip olduğunu göstermiştir. Hücre proliferasyon ve canlılık testleri fiberler üzerine birincil insan keratinosit hücrelerinin ekimi ile gerçekleştirilmiştir. PCL/İF karışımı olan

fiberlerde sadece PCL ve sadece İF olan fiberlere göre daha iyi proliferasyon ve canlılık olduğu gözlenmiştir.

ACKNOWLEDGEMENTS

First of all, I would like to express my sincerest gratitude to my supervisor Prof. Dr. Yusuf Z. Menceloğlu for his support and valuable advice during my master's study. I would also like to thank my thesis juries: Assoc. Prof. Yavuz E. Arslan for his valuable guidance and support throughout my experiments and Assoc. Prof. Burak Derkuş for improving the value of my studies by carrying out the in vitro experiments of this project.

I am grateful to TUBITAK 1004 for granting this project entitled "Mikrobiyota Kaynaklı Post-biyotik Mediatör Destekli İnsan Epidermal Doku Eşdeğerinin Vücut Dışında Üretilmesi: Rejeneratif Tıp Uygulamaları için Yeni Bir Doku Mühendisliği Ürünü'' Number: P4 - 20AG030. I also want to thank Doç. Dr. Gürkan R. as the leader of this project.

I am grateful to have precious friends with me on campus who allowed me to have one of the greatest times of my life: Büşra Elif Kıvrak, Aybüke Büşra Özer, Gülnur Şener, Cemile Uslu, Sümeyye Narin, Beril Üstünkaya, Belkıs Güneş, Eda Güney, and Melike Nur Önder, and Forough Mahdipour.

I would like to thank my lab members Ogeday Rodop, Aybike Mine Ersin, Gizem Kurtulmuş, Gizem Arıtürk, Gökmen Taner Şanlı, Çağla Girişken, Elif Daldal, Hatice İlgen for their support in the lab.

I am grateful to my teacher Assist. Prof. Erinç Bahçegül who has been a valuable mentor for me since my bachelor's and a great role model. I am thankful to him since he always makes me feel like my every achievement is valuable and always believes that I will be a successful researcher.

My best friend, Beyza Nur Kaya, was always there for me since high school, has listened to my worries countless times, and always encouraged me to follow my dreams. Thank you for always being by my side.

Finally, and most importantly, this journey would not be possible without my dear family who always supported me in every decision I made and comforted me in the tough times. Thank you for always supporting me to follow my dreams despite every hardship. I love you so much!

TABLE OF CONTENTS

LIST of FIGURES

LIST OF TABLES

LIST of ABBREVIATIONS

PCL – Polycaprolactone

SF - Silk Fibroin

SEM – Scanning Electron Microscopy

ECM – Extracellular matrix

PVA – Polyvinyl acetate

PEG - Polyethylene glycol

PVA - Polyvinyl alcohol

PPF - Poly(propylene) fumarate

PU - Polyurethane

PMMA - Poly methyl methacrylate

PS - Polystyrene

HNT - Halloysite nanotube

PVP - Polyvinyl pyrrolidine

PVB - Polyvinyl butyral

FGF1 - fibroblast growth factor 1

INS – Insulin-loaded SF sponge

HFIP - Hexafluoroisopropanol

PS1 - PCL: SF (7:3)

PS2 - PCL: SF (3:7)

PS2PS1 - PCL:SF (3:7) on PCL:SF (7:3)

FTIR - Fourier transform infrared spectroscopy

SDS-PAGE - Sodium dodecyl sulfate-polyacrylamide gel electrophoresis

TGA - Thermal Gravimetric Analysis

BET - Brunauer–Emmett–Teller

BJH - Barrett-Joyner-Halenda

μm - Micrometres

°C - Degrees centigrade

μl - Microlitres

v/v - Volume per volume

w/v - Weight per volume

1. Introduction

1.1.Skin structure and wound formation

The skin constitutes the largest organ of the human body and protects the body like a barrier against external impacts. The skin has vital functions such as the regulation of temperature and protection against UV light, microorganisms, trauma, toxins, and pathogens. It also serves roles such as controlling fluid loss and homeostasis and takes part in immunologic observation and sensory inspection. The structure, thickness, and functions of the skin vary in different body parts [1].

The skin comprises three main layers: epidermis, dermis, and subcutaneous tissue, from the outer to the inner layer, respectively. The structure of the skin is given in Figure 1 [2]. The epidermis acts as a water and microbial barrier and provides the skin tone. The dermis is the middle layer and is made up of connective tissue, lymphatic vessels, blood vessels, hair follicles, and sweat glands. The inner subcutaneous tissue is composed of connective tissue and fat [3].

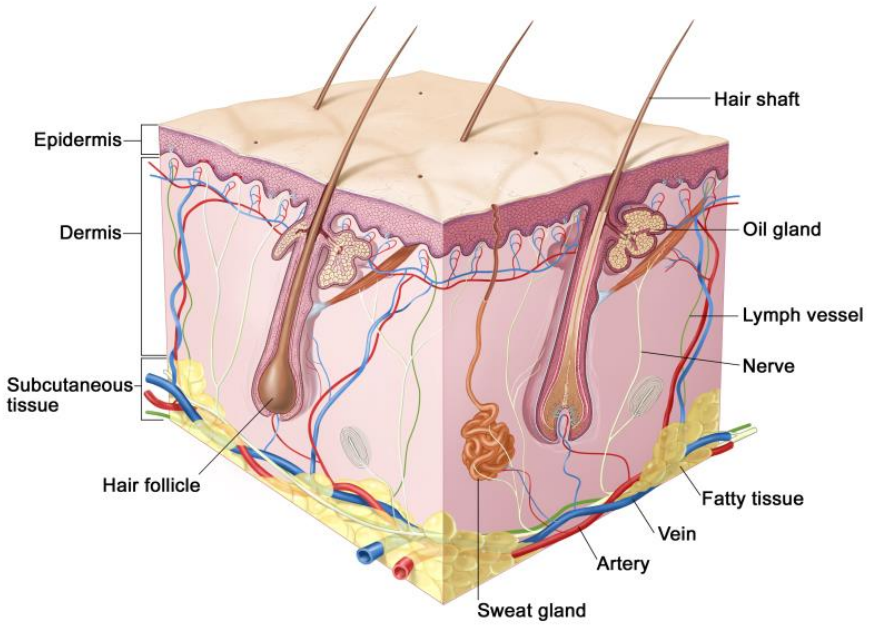

Figure 1 Structure of the skin [2].

Wound formation causes the interruption of skin integrity, and it could result from thermal or mechanical damage. The healing time of these wounds categorizes them into two types: acute wounds and chronic wounds. Acute wounds regain their previous integrity after some time, whereas chronic wounds continuously experience inflammation, necrosis, and non-healed open wounds [4].

Wound healing consists of four stages which are hemostasis, inflammation, proliferation, and remodeling. At the beginning of the wound formation, platelets and inflammatory cells move into the wound site where the extracellular matrix is exposed to its collagen. The next step is inflammation which takes around 72 h. In this step, mast cells release enzymes, histamine, and amines into the wound site. Later, proliferation begins to take place with a decreased rate of inflammation. The wound site is reconstructed with fibroblast proliferation and collagen deposition. The proliferation step involves several occasions such as tissue granulation, re-epithelialization, neovascularization, and wound contraction. Finally, the migration of cells into the wound area takes place which allows the remodeling and regeneration of the site.

1.2.Electrospinning

Electrospinning is a technique that is widely used to produce materials with nano to micron-size fibers by the application of an electrical field to the ejected polymer solution. The electrospinning technique was first used around the 1930s and was patented by Formhals. Electrospinning is very useful to produce materials with a high surface area-to-volume ratio and small pore size [5]. The technique has been used in several areas such as tissue engineering, agriculture, textile, and aerospace engineering,

Electrospinning requires a polymer solution, a collector, and a high-voltage supply. The applied voltage between the nozzle and the collector creates a microsphere at the tip of the nozzle. This microsphere is pulled from the tip, and it elongates because of the adjacent charges in the same jet. Polymer solution forms a cone called Taylor's cone before leaving the tip of the needle which allows adequate fiber formation [6]. The formed jet gets exposed to bending instabilities and fiber whipping resulting in the randomly formed nanofibers on the collector. As fibers are collected on the collector, the solvent is evaporated, and the final material is formed.

It is possible to spin most of the polymers if a proper solvent is chosen. Evaporation of the solvent, solubility, and the concentration of the polymer solution affect the morphology of the fibers [7]. The electrospinning process is given in Figure 2 [8].

Electrospinning has several advantages over production techniques such as low cost, improved production rate, high control over the system, production of scaffolds with high surface area and small pore size, and high filtration efficiency [9]. Providing scaffolds with a high surface area enhances cell proliferation, attachment, differentiation, and migration through the material leading to high cellular activity [10]. In addition, electrospun nanofibers create a structure that could mimic the extracellular matrix (ECM) of the tissues and resulting in improved cellular functions in the scaffolds. ECM takes a great role in ECM-cell interactions, which allows the transduction of information along the tissues [11][12]. Electrospinning involves some drawbacks as well like the use of toxic solvents with high volatility, jet instability, and strength of the web.

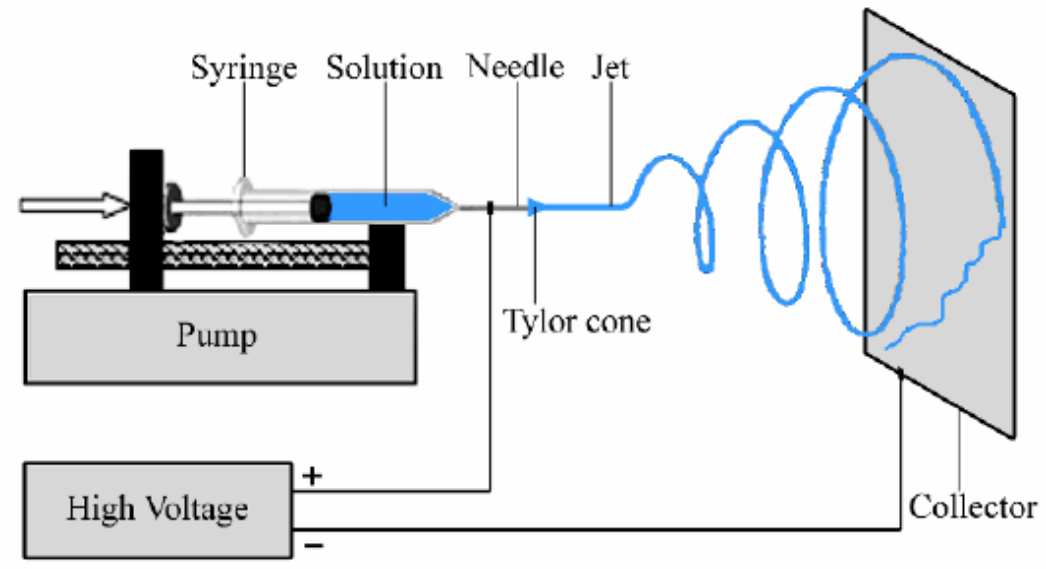

Figure 2 Electrospinning setup and Taylor's cone formation [8].

1.3. Current studies for skin scaffolds

As the wound treatment and rehabilitation of wounds are expensive, possible new treatments are being investigated for the mitigation of inflammation especially in wounds that are more exposed to infections. Dressings are the major focus for wound treatment, and they are proven to be very useful. Dressings are successful in the promotion of cell and tissue regeneration, control of microbial activities, and providing surface defense [13].

The classical approach dressings are the ones utilized in hospitals for full-thickness skin wounds or burns. Skin grafts are categorized into four categories: skin substitutes, autografts, allografts and xenografts.

Autografts are the type of skin tissues that are harvested from the undamaged part of the skin from the patient's own body and applied to the wound site. Autografts are very significant in the wound healing field due to their low-to-nonimmune responses as they are from the same patient. This property makes them the gold standard in the treatment of full-thickness skin wounds, especially high-degree burns. However, the new wound formation and the limited availability of autografts restrict the use of these grafts [13][14].

Allografts are great alternatives to autografts where they temporarily protect the wound area from fluid loss and contamination by bacterial species. These grafts are taken from a patient and applied to the other one. However, they also contain problems such as the probability of immune rejection, since implanted from another person, and infection [15].

Xenografts are the final graft type, and they are taken from another species. They also possess problems similar to allografts such as a high probability of immune rejection and being only a temporary solution. So they are mostly used as protective layers previous to treatments [16].

Skin substitutes are promising alternatives to grafts that are produced in laboratory environments. Skin substitutes are produced in a way to mimic the extracellular matrix in 3D form to promote cell migration and proliferation leading to improved wound healing process. Biomaterials are chosen and generated in a way to provide good biocompatibility, antibacterial activity, and enhanced wound healing. Polymeric materials

are commonly used as dressings because of their special role in drug delivery and tissue engineering functions and ease of dressing fabrication [17].

1.4.Polymer-based skin scaffolds

Over the previous years, various types of polymers which are natural, synthetic, or hybrid have been used for skin engineering applications and are even available on the market.

Natural polymers are obtained from natural resources and provide bioactivity, and a biomimetic environment to tissues and cells. They are mostly chosen because of their superior properties such as biodegradability, biocompatibility, nontoxicity, and resemblance to the natural environment [18]. Natural polymers could be categorized into two branches: Polysaccharide-based polymers such as cellulose, agar, hyaluronic acid, dextran, starch, and protein-based polymers such as collagen, silk, elastin, keratin, and fibrin [19][20].

In one study, Wang et al. produced a dextran-based hydrogel that can take the shape of the applied wound site. As the hydrogel filled the whole wound site without leaving a gap leading to accelerated wound healing [21].

As they possess active functional groups natural polymers could be modified to become more effective wound healing agents. For example, Liang et al. recently introduced a quaternized chitosan hydrogel that is highly water soluble and with antibacterial activity [22].

In another study, Zhang et al. used both polyvinyl acetate (PVA) and gelatin methacrylate (GelMA) to form a microneedle scaffold. Microneedles were loaded with hemoglobin and phosphorus quantum dots which showed a near-infrared light-responsive oxygen release leading to enhanced chronic wound healing [23]. Gao et al. provided a biodegradable hydrogel scaffold formed from ε-Poly-L-Lysine and dextran with the property of antibacterial activity against microorganisms [24].

In a recent study, Hu et al. produced a film-casted chitosan dressing for second-degree deep burns and showed that it could decrease the healing time of the wound and mitigate the wound pain during healing [25].

Synthetic polymers are prepared with hydrocarbon building blocks in a laboratory environment. They are highly preferred in various fields as they can be produced in different forms and designated structures. However, their main drawback is their lack of cell adhesion sites and the requirement for functional modification for improved cellular functionality [26] [27]. Synthetic polymers are mostly examined under two sections: Degradable synthetic polymers and non-degradable synthetic polymers.

Degradable synthetic polymers could be broken down into simpler structures and the most common ones are polyethylene glycol (PEG), polyvinyl alcohol (PVA), polycaprolactone (PCL), and poly(propylene) fumarate (PPF). Non-degradable polymers are not able to degrade into simpler forms by biological factors and the most known examples are polyurethane (PU), poly methyl methacrylate (PMMA), and polystyrene (PS).

In a recent study, Mohebali et al. created a nanocomposite film composing PVA and halloysite nanotube (HNT) for the delivery of minocycline. It was found that the nanocomposite provides successful monocyte delivery for bacterial inhibition. In burn wounds [28]. Zehra et al. introduced an electrospun PCL/sodium percarbonate oxygen-releasing system which caused enhanced angiogenesis and increased protein production [29]. Liu et al. produced an electrospun system with polyvinyl pyrrolidine (PVP)/polyvinyl butyral (PVB) which improved the air permeability, antibacterial property, and wound healing efficiency [30].

Hybrid polymers are a promising area of research that involves blending natural and synthetic polymers to take advantage of both their properties and minimize their drawbacks [31].

For instance, Viezzer et al. produced a Chitosan/PU-based hydrogel that improved the wound healing process in diabetic rat models with minimized toxicity [32]. Abbasi et al. created a hydrogel system with Alginate/PVA which inhibits bacterial species such as S. aureus and P. aregnosa. Hydrogel also showed accelerated wound closure, improved granulation, and re-epithelization of tissues [33]. In another study, Gsib et al. proposed a copolymerized PEG/fibrin scaffold model that improved cellular infiltration, and tissue remodeling and provided a system with adjustable properties [34].

1.4.1. PCL-based skin scaffolds

Polycaprolactone is a synthetic polymer that is made up of hexanoate units and it is under the category of aliphatic polyesters. The structure of PCL is given in Figure 3 [35]. Owing to its biodegradable nature, it became very popular in wound healing applications. PCL has several advantages such as advanced mechanical properties, biocompatibility, and the ability to become miscible with several polymers [36].

Powell et al. produced a skin substitute with PCL and collagen, and it was shown that the addition of PCL improved the material stiffness which made it easier for surgeons to handle [37].

Ghomi et al. created a PCL/gelatin electrospun where PCL was used to improve the mechanical properties of the overall scaffold [38]. In another study, Metwally et al. created PCL patches from electrospun with random and aligned fibers by both increasing the mechanical properties and natural oil carrying capacity [39].

Even though PCL is a great polymer for tissue engineering applications, instead of using it by itself blending it with a natural polymer would provide a better environment for cell growth by improving the hydrophilicity and attachment to the functional groups.

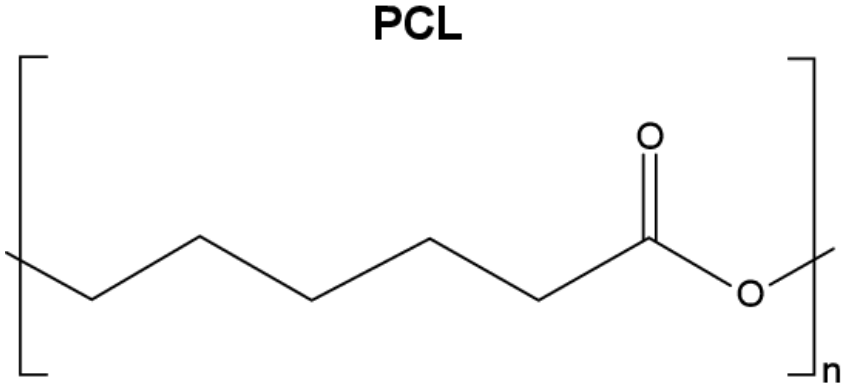

Figure 3 Structure of PCL [36].

1.4.2. SF-based skin scaffolds

Silk is a natural polymer, also a protein, that is widely used in medical applications. The structure of SF is given in Figure 4 [40]. Silk fibroin possesses a function to activate the body's immune response. It also has enhanced properties such as biocompatibility, low immunogenicity, and gradual disintegration. Silk fibroin improves stem cell adhesion, differentiation, and propagation. Additionally, promotes tissue regeneration and prevents adherence of pathologic microorganisms onto the tissue[41].

In one study, Ju et al. demonstrated that SF electrospun enhances the re-epithelization of the wound site and accelerates wound closure, especially in burn wounds. According to the expression analysis, they suggested that the SF electrospun mitigates inflammation and scar formation [42][43].

Guo et al. investigated SF electrospun with random and aligned fibers and their effect on wound healing and vascularization in Sprague-Dawley rats. In vivo analysis showed that both scaffolds have strong contributions to epithelialization in full-thickness wounds [44].

Similarly, Sirong He et al. immobilized heparin in SF hydrogels containing acidic fibroblast growth factor 1 (FGF1) and their impact on wound healing in Sprague-Dawley rats. They proved that SF hydrogels enhanced cell proliferation and migration of the L929 cell line [45].

In another study, Ju et al. compared the effect of SF nano matrix and a commercial polyurethane-based dressing called Medifoam on a second-degree burn. It was investigated after seven days that the wound closure of SF electrospun treated wound is greater than Mediforam treated wound. Additionally, the wound size decreased to 4% with SF electrospun and to 8% with Medifoam at the end of the 28^{th} day. Histological analysis showed that re-epithelialization and regeneration of skin highly increased with the treatment of SF electrospun. It was also examined that the expression of pro-inflammatory factors such as IL-1$\propto$ and IL-6 significantly decreased [42].

SF-based biomaterials have also become promising for diabetic wound healing. Yang et al. conducted a study on diabetic Sprague-Dawley rats using insulin loaded SF sponge (INS). They concluded that the insulin-loaded SF sponge showed an enhanced rate of

wound healing. SF sponge without insulin also improved wound healing compared to untreated wounds [46].

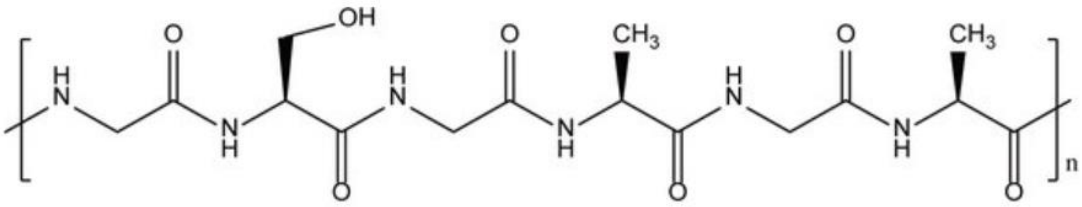

Figure 4 The structure of SF [40].

1.5. Objective of the Study

In this study, it was aimed to produce a polymer nanofiber system that can substitute the epidermal layer by providing improved and scarless healing. For this purpose, the electrospinning method was chosen since it allows the construction of scaffolds with a high surface area to volume ratio and small pore size which enhances the attachment and the proliferation of cells.

The polymer system was constructed with two polymers, which are PCL and SF. PCL possesses several advantageous properties such as high mechanical strength, biocompatibility, and non-toxicity. However, it also has some disadvantages such as hydrophobicity, slow biodegradation, and deficiency in cell recognition sites. SF is a widely used natural polymer with high hydrophilicity, improved oxygen and water uptake, and low immunogenicity, whereas it suffers from low mechanical strength and a limited number of solvents for the electrospinning of SF. In this system, PCL and SF were blended in different ratios to assess the most suitable scaffold structure. This system allowed us to combine the advantageous properties of both polymers by compensating for their individual drawbacks. SF was utilized for its hydrophilicity and presence of recognition sites which induce cellular proliferation. PCL was used for its high integrity and mechanical strength. Here, we assessed the characteristics of PCL/SF nanofibers such as mechanical strength, fiber morphology, thermal stability, surface area, pore size, degradation, contact angle, and cytocompatibility.

2. Materials and Methods

2.1.Materials

Silk fibroin (SF) extracted from Bombyx mori cocoons was provided from Bursa Kozabirlik, Turkiye. Polycaprolactone (PCL) (M_w= 80,000), Na_2CO_3, LiBr, Dialysis tubing cellulose membrane (Molecular weight cut-off = 14,000), Hexafluoroisopropanol (HFIP), Proteinase K from Tritirachium album (≥30 units/mg protein), Calcium chloride, Gentamicin and Trypsin solution was purchased from Sigma Aldrich, U.S. Amphotericin B was provided from Life Technologies, Grand Island, NY. T-75 flask was purchased from Corning, NY.

2.2. Extraction of silk fibroin from the B. mori

The extraction of SF was performed using the related Nature protocol [47]. The process followed for the extraction of SF is depicted in Figure 5. In summary, cocoons were divided into smaller parts, and they were boiled in 0.02M Na_2CO_3 solution for degumming. Then, fibers were rinsed in ultra-pure distilled water from any salt and impurity for 20 minutes 3 times. Purified fibers were dried in a hood overnight. In the next step, 2.5 grams of dried fiber were soaked with 10 mL of 9.3 M LiBr solution in a small beaker. The beaker was put in an oven at 60°C and dissolved for 4 hours.

The fibrous solution was put in a dialysis bag inside 1 L of ultra-pure distilled water. The dialysis took 2 days with the water changes after 1 hour, after 4 hours, in the evening, the next morning, the next evening, and lastly the next morning (6 times overall). After the completion of 24 hours, the dialysis was ended, and the fibroin solution was centrifuged for 10 minutes at 4°C and 2000 rpm. For the prolonged storage of the silk fibroin, the solution was freeze-dried for 2-3 days to get rid of any water present.

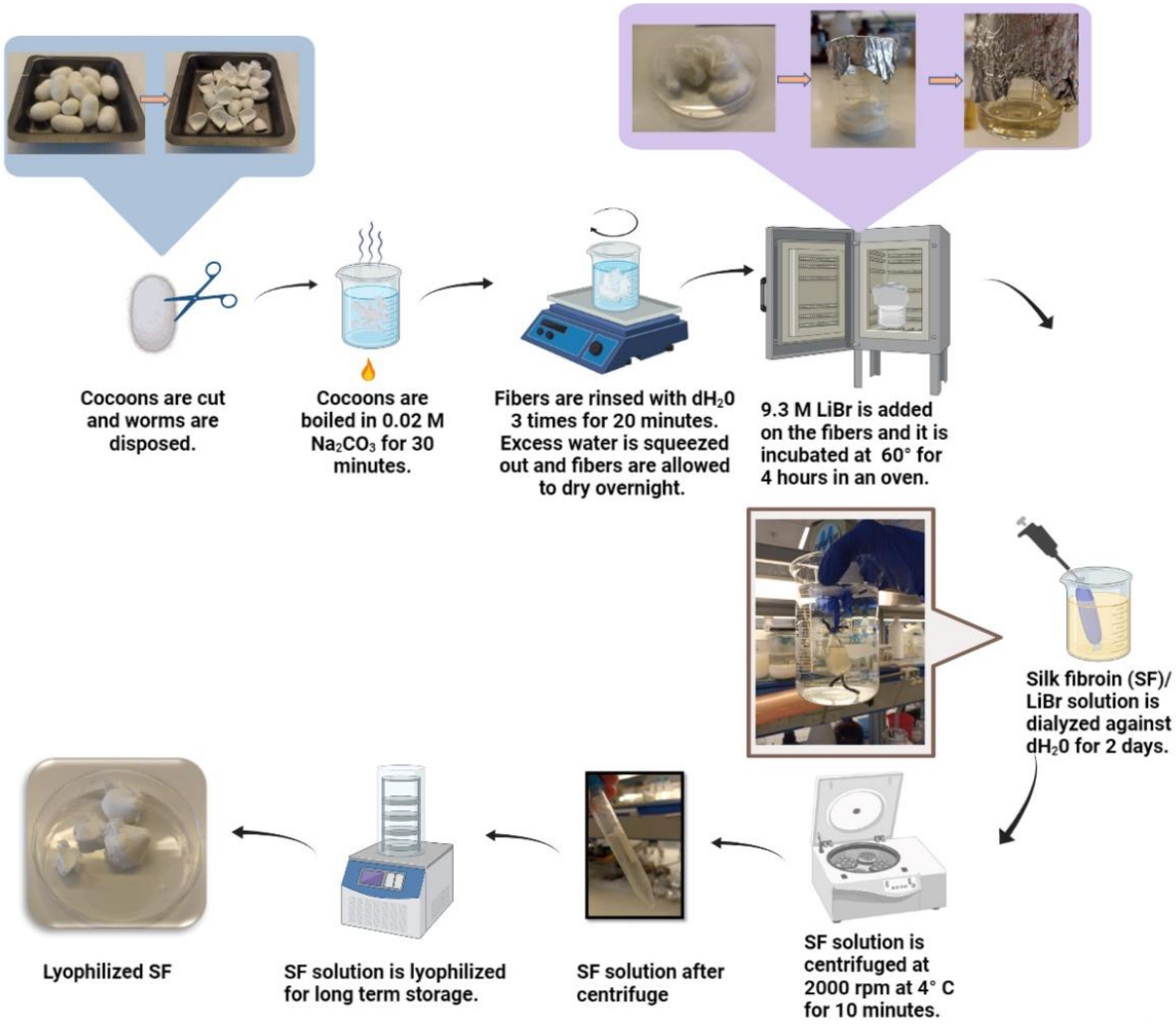

Figure 5 Silk Fibroin extraction process.

2.3.Preparation of the polymer solutions

The polymer nanofibers prepared in this project involve two major polymers which are PCL and SF. Polymer solutions were prepared by dissolving 10% (w/v) PCL and 5% (w/v) in HFIP separately and in blended forms. There are 5 polymer films prepared which are 5%SF (SF), 10% PCL (PCL), PCL: SF mixed in 7:3 volume ratio (PS1), PCL: SF mixed in 3:7 volume ratio (PS2), and PS1 electrospun on PS2 electrospun (PS2PS1). Layer-by-layer nanofibers were prepared by first electrospinning one polymer solution on an aluminum foil and then the other polymer solution on top of it.

2.4. Preparation of the polymer nanofibers

The electrospinning process was carried out by using the Apparatus of New Era Pump Systems, Inc. device. The electrospinning set-up used for this project is depicted in Figure 6. Before electrospinning, the polymer solution was filled into a 5 mL syringe, and an 18-gauge needle tip (KRUUSE, Denmark) was used. To collect the polymer nanofibers easily, the metal collector was covered with aluminum foil. Then, an electrical field was applied between the needle tip and the metal collector. Electrospinning parameters are given in Table 1.

During the electrospinning, the polymer solution was ejected from the needle tip in nanofiber form, and the solvent evaporated and collected onto the aluminum foil. Parameters used for the electrospinning of the polymer fibers are given in Table 1. Since the nanofibers formed from silk fibroin are water soluble, they require an additional treatment after the fabrication. Polymer fibers were treated with 99% methanol for 30 minutes and rinsed with distilled water several times to turn the fibers from water-soluble to water-insoluble.

Figure 6 Electrospinning set-up used to produce nanofibers.

Table 1 Electrospinning parameters of the polymer nanofibers

Polymer nanofiber	**Concentration (w/v)**	**Feed rate (mL/h)**	**Collector distance (cm)**	**Voltage (kV)**
PCL	10%	1.5	15	12
SF	5%	1.5	10	11
PS1	10% PCL:5%SF (7:3)	1.5	10	7
PS2	10% PCL:5%SF (3:7)	0.6	10	6
PS2PS1	10% PCL:5%SF	0.6-1.5	10-10	6-7

2.5. Extraction of Primary Human skin keratinocytes

The University of KOC Institutional Review Board approved the use of skin tissues from the patients, and an informed agreement form was obtained for the donors for research purposes. Full-thickness human epidermal tissues were obtained from 2 patients who underwent breast reduction surgery. The method that was established by Marcelo et al. was followed for the establishment of keratinocyte cell strains [48][49]. In short, skin tissues were digested in a 0.125% trypsin solution overnight at room temperature. Enzymatically dissociated tissues were seeded 30 to 40 x 1000000 cells per T-75 flasks. Cells were cultured in a chemically defined serum-free medium containing 0.06-mmol/L calcium chloride, 0.375-mg/mL amphotericin B, and 25-mg/mL gentamicin. Primary keratinocytes were harvested and subcultured subsequently when they were 70% to 80% confluent.

2.1. Characterization of the polymer nanofibers

2.2.1. Fourier transform infrared spectroscopy

Structural analysis of SF was conducted using Fourier transform infrared spectroscopy (FTIR, Shimadzu-Infinity spectrometer, Japan). This method allowed the detection of the amide bonds that are characteristic of SF which proves the successful extraction of SF from B. mori cocoons. FTIR analysis was performed with a resolution of 2 cm^{-1} in the range of 4000-500 cm^{-1} at room temperature.

2.5.1. Sodium dodecyl sulfate-polyacrylamide gel electrophoresis

Sodium dodecyl sulfate-polyacrylamide gel electrophoresis (SDS-PAGE) was used to determine the molecular weight of the extracted SF by following the Laemmli (1970) method with 5% condensing gel and 10% resolving gel [50]. In short, the loading buffer was mixed with SF solution, and it was exposed to hot water for a short time. Prepared

samples were added into wells and electrophoresis was conducted for approximately 1.5-2 hours under 20 mA current at first and under 40 mA current until the end. Lastly, the molecular weight of the SF was determined by examining the electrophoretic profiles of SF with the standard protein ladder.

2.5.2. Scanning Electron Microscopy (SEM)

Morphological analysis of polymer nanofibers was performed using Scanning Electron Microscopy of LEO Supra 35 VP microscope (Zeiss, Oberkochen, Germany) after gold/palladium coating of samples. ImageJ software was used to determine mean fiber diameter and fiber diameter distribution by measuring at least 80 random fibers for each sample.

2.5.3. Mechanical Test Analysis

Mechanical properties of nanofibers were conducted using a mechanical tester (UniVert, CellScale Biomaterials Testing) with a strain rate of 0.3 mm s^{-1}. Analysis was carried out at least two times for each sample at room temperature conditions with the 2 cm x 5 cm dimensions.

2.5.4. Thermal Gravimetric Analysis

The thermal Gravimetric Analysis (TGA) method was used to determine the time-dependent weight loss and the thermal stability of the samples. The analysis was conducted by raising the system temperature from 30°C to 600°C with a ramp rate of 10.00°C/min under the nitrogen gas with the TGA device (Perkin Elmer, Waltham, MA, USA).

2.5.5. Water Contact Angle Test

The hydrophobicity/hydrophilicity of samples was determined with the water contact angle test using a Drop Shape Analyzer 10 MK2 device (KRUSS, Hamburg, Germany). On each sample 5 μL water was dropped using the sessile drop method and water contact angles were calculated afterward.

2.5.6. Brunauer–Emmett–Teller Analysis

The surface area, pore volume, and pore size of the samples were measured with the Quadsord SI 5 Brunauer–Emmett–Teller (BET) device (Quantachrome Instruments, Anton-Paar GmbH, Graz, Austria) using the Barrett-Joyner-Halenda (BJH) analysis method. Each analysis was performed under a liquid nitrogen environment (77K) with the 0.01–0.99P/P0 pressure range and a nitrogen adsorbate gas.

2.5.7. In vitro degradation analysis

In vitro degradation study of the samples was conducted using the Proteinase K enzyme. 0.01% (w/v) Proteinase K was prepared in a 0.02 M Tris-HCL buffer with pH=8 and 0.01% (w/v) sodium azide was added into the overall buffer to avoid microbial growth. Each sample was cut into pieces with an approximate weight of 4 mg with 3 replicates. Each sample was put into a 5 mg buffer solution with enzyme and incubated at 37 °C. The samples were incubated for 12 h and 24 h. After the experiment, each sample was centrifuged 2 times and washed with distilled water. Finally, samples were freeze-dried and the degradation percentages were calculated after the weighing.

2.5.8. Cell Proliferation and Viability

Live/dead and XTT assays were conducted to determine the cytotoxicity of the scaffolds in terms of cell viability and proliferation. Primary human epidermal keratinocyte cells (40,000 cells/nanofiber) were seeded on the polymer nanofiber samples for the assessment of cell viability and proliferation. Cells were cultured for 7 days and, the imaging of the live and dead cells was performed using the calcein-AM (4 μM, Molecular Probes, Thermo Fisher, UK) and ethidium homodimer-1 (EthD-1, 2 μM, Molecular Probes, Thermo Fisher, UK) stains, respectively. Cells were monitored under fluorescent microscope (Leica DMIL, Germany) by using the 488 nm (green) and 527 nm (red) wavelengths. The proliferation rate of the cells in each sample was conducted by XTT (Biological Industries, USA) assay. After 7 days of culturing the primary human epidermal keratinocyte cells were rinsed and XTT reagent (50 μL) was incorporated into samples.

2. Results and Discussions

2.1. Characterization of the SF solution

To determine the successful extraction of SF from B. mori cocoons, several characterization techniques were used. First, FTIR analysis was conducted for the structural characterization of the extracted SF. SF contains various characteristic amide bonds in its structure and by detecting these amide bonds the validation of the successful extraction could be proven. Figure 7 depicts the SF peaks from the FTIR spectrum. All the peaks were compatible with the literature where the 1642 cm^{-1} peak represents the Amide I band which comes from the C=O bond formed in the β-sheet region of the SF. The Amide II band was detected from the 1517 cm^{-1} peak in the spectrum and this band corresponds to CN stretching and NH deformation in the β-sheet region of the SF. Amide III band was observed in 1232 cm^{-1} in between α-helix/random coils and β-sheet from C-N stretching. Lastly, the 3282 cm^{-1} peak represents the Amide A band with NH bending in the β-sheet region [51][52].

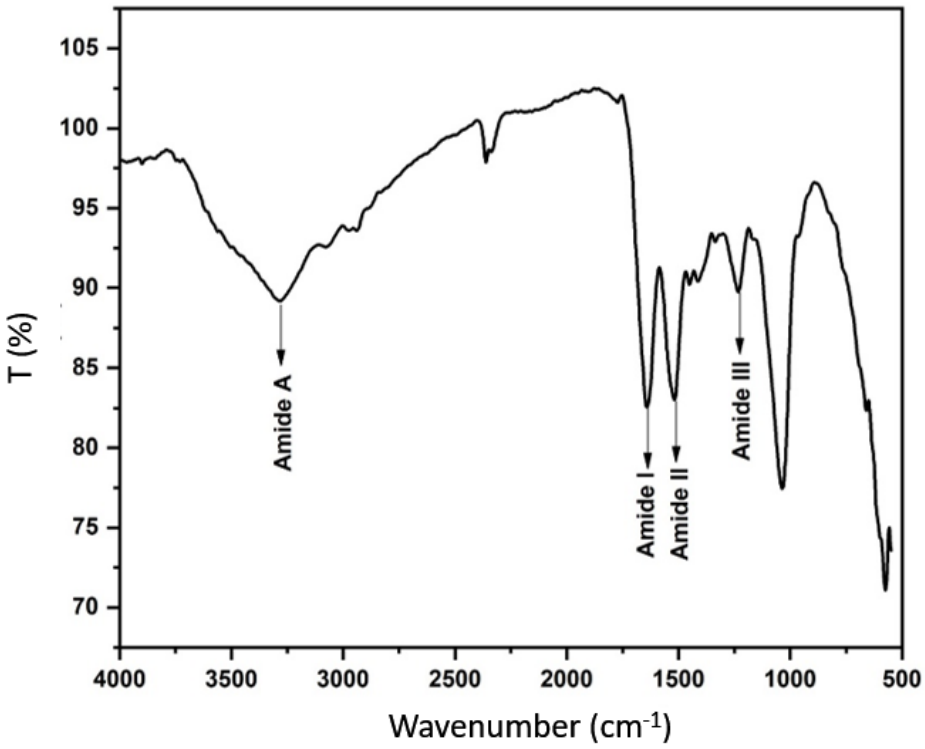

Figure 7 FTIR spectrum of the SF.

Molecular weight determination of SF is important to specify the accurate degradation of SF during extraction and the electrospinning property of SF. SDS-PAGE electrophoresis analysis was used to identify the molecular weight of the extracted SF. SDS-PAGE gel showing the SF molecular weight compared to the standard protein ladder is shown in Figure 8. On the other hand, the SF column gave a smeared staining from around 60 kDa to 250 kDa and it even exceeded the 250 kDa level. It indicates that extracted SF had chains with molecular weight ranging from 60 kDa to over 250 kDa. It is stated in the study proposed by Rockwood et al. that when a cocoon is degummed for 30 min, silk fibroin possesses a molecular weight of around 100 kDa which is correlated with the results of this study [47].

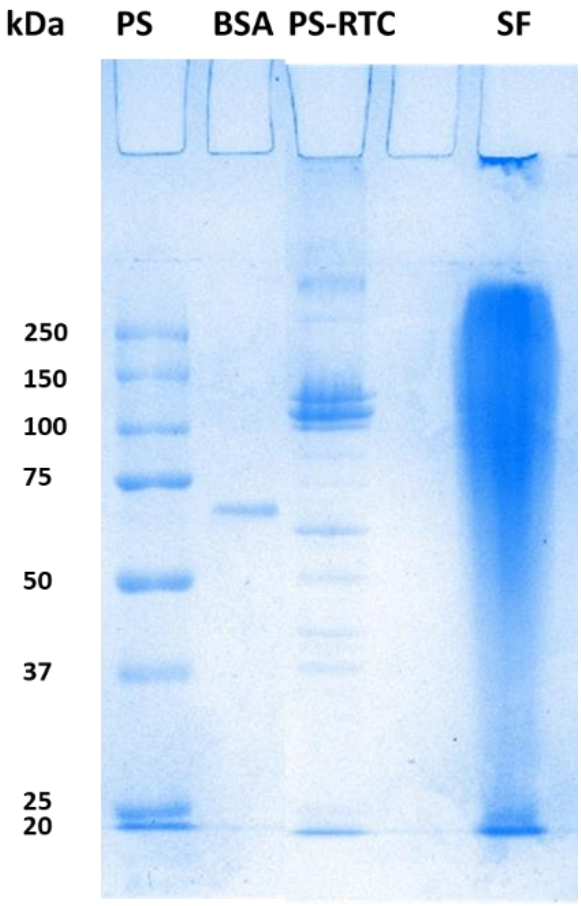

Figure 81 SDS-PAGE analysis of SF.

2.2. Morphological Characterization of the polymer nanofibers

One of the most important challenges of scaffold production is the generation of structures that resemble the native extracellular matrix of living tissues and organs. So, determining the morphology of scaffolds is significant to evaluate their capability to support seeded cells and to guide the cells for improved proliferation [53]. SEM analysis was used to determine the morphology of nanofibers and their fiber diameters. Figure 9 illustrates the SEM images of the scaffold and gives the fiber diameter distribution of polymer nanofibers. As can be seen, all nanofibers were produced homogenously and none of the scaffolds showed bead formation.

Like most natural polymers, SF is not easy to spin, and finding the appropriate solvent system is challenging. However, in our system, SF was homogenously dissolved in HFIP and easily spinned by producing well-distributed nanofibers [54][55]. HFIP was also used

for the solvent system of PCL, and it allowed the easy blending of the SF and PCL in various ratios. Using HFIP solvent allowed the production of more concentrated polymer solutions leading to having more control over the fiber diameter and fiber diameter distribution [56]. Nanofibers produced from pure PCL showed thicker fibers with a mean fiber diameter of 1.582 ± 0.246 μm (Figure 9a). It also demonstrated comparably nonuniform distributions in terms of fiber diameter. On the opposite, the thinnest fibers were obtained with pure SF electrospinning with a mean diameter of 0.408 ± 0.125 μm (Figure 9b). This could be the result of the low viscosity of the SF polymer solution and the high conductivity resulting from the nature of bioactive SF [57].

Overall, the thickest fibers were observed in PS1 with a mean fiber diameter of 2.236 ± 0.842 μm and it showed the highest fiber diameter distribution difference (Figure 9c). Unexpectedly PS1 had a greater fiber diameter than pure PCL. The reason could be that lower voltage was applied to PS1 during electrospinning compared to that of PCL [58]. PS2 contained thin fibers with 0.473 ± 0.106 μm (Figure 9d) since the SF ratio was higher in composition compared to that of PS1. Additionally, PS2PS1 was made up of 1.542 ± 0.498 μm fiber diameter which was formed from both fiber layers PS1 and PS2 (Figure 9e).

In one study, by Gandhimathi et al. observed that SF addition into the PCL structure created thinner fibers where the diameter decreased from 215 nm to 164 nm under similar electrospinning parameters [59]. This study supports the idea that the addition of SF produces fibers with smaller diameters. Similarly, in our study, SF produced thinner diameters compared to PCL when the parameters were kept almost constant. However, PS1 did not follow the same effect and the diameter of the fibers got thicker after the addition of SF into PCL. The reason is that PS1 was constructed using low voltages compared to PCL and SF samples, which led to thicker fibers than expected. So, it could be stated that the addition of SF into PCL cannot be evaluated separately without taking the other parameters, such as voltage, the distance between the needle tip and the collector, and the feed rate, into consideration.

2.3. Thermal Gravimetric Analysis

TGA was performed to analyze the thermal stability and temperature-dependent weight loss of the samples. Analysis was conducted between the temperatures of 30°C and 600°C with a temperature increase of 10.00°C/min under a nitrogen atmosphere. Figure 10 shows the time-dependent weight loss of samples.

Each sample experienced an initial weight loss caused by water evaporation except for the PCL sample [60]. Water loss of each sample was as follows: 20% from SF, 5% from PS1, 13% from PS2, and 8% from PS2PS1. It is observed that in correlation to the PCL amount in the scaffold, the water loss percentage decreases with increasing PCL amount. This could be a result of the hydrophilic nature of SF which holds water in interaction with the -OH groups compared to the lack of hydrophilic groups in PCL structure. SF curve had a weight loss at 300 °C due to the decomposition of SF macromolecules [61] and PCL experienced a rapid decomposition at the temperature of 400 °C.

Prepared samples formed from the blend of the two polymers showed decompositions at both temperatures of 300 °C and 400 °C in proportion to the amount of the polymer type contained. For instance, PS1 showed a weight loss of 23% between the temperatures 300 °C-400 °C, and a weight loss of 66 % after 400 °C. PS2 experienced a weight loss of 26 % between the temperatures 300 °C-400 °C, and a weight loss of 45% after 400 °C. As can be seen, the SF amount is directly correlated with the weight loss percent between 300 °C and 400 °C. PS2PS1 scaffold possessed similar weight decomposition rates with PS1.

Bajsić et al. examined the decomposition process of PCL/SF nanofibers and observed 3-step weight losses. These 3 steps were before 100 °C, between 100 °C and 350 °C, and after 350 °C which were associated with water evaporation, SF decomposition, and PCL decomposition, respectively [62]. In another study, Luo et al. examined the thermal characteristics of SF/Polyurethane fibers and stated that the weight loss between 250-400 °C was associated with the decomposition of SF macromolecules [60].

The total weight losses of the samples are given in Table 2. The highest weight loss belonged to PCL with 99.41 % and the lowest weight loss was observed in SF with 64.33%. It can be stated that SF had better thermal stability compared to PCL [60].

Therefore, the amount of decomposition increased with the increasing PCL content. In addition, SF had the highest char yield compared to other scaffolds [63].

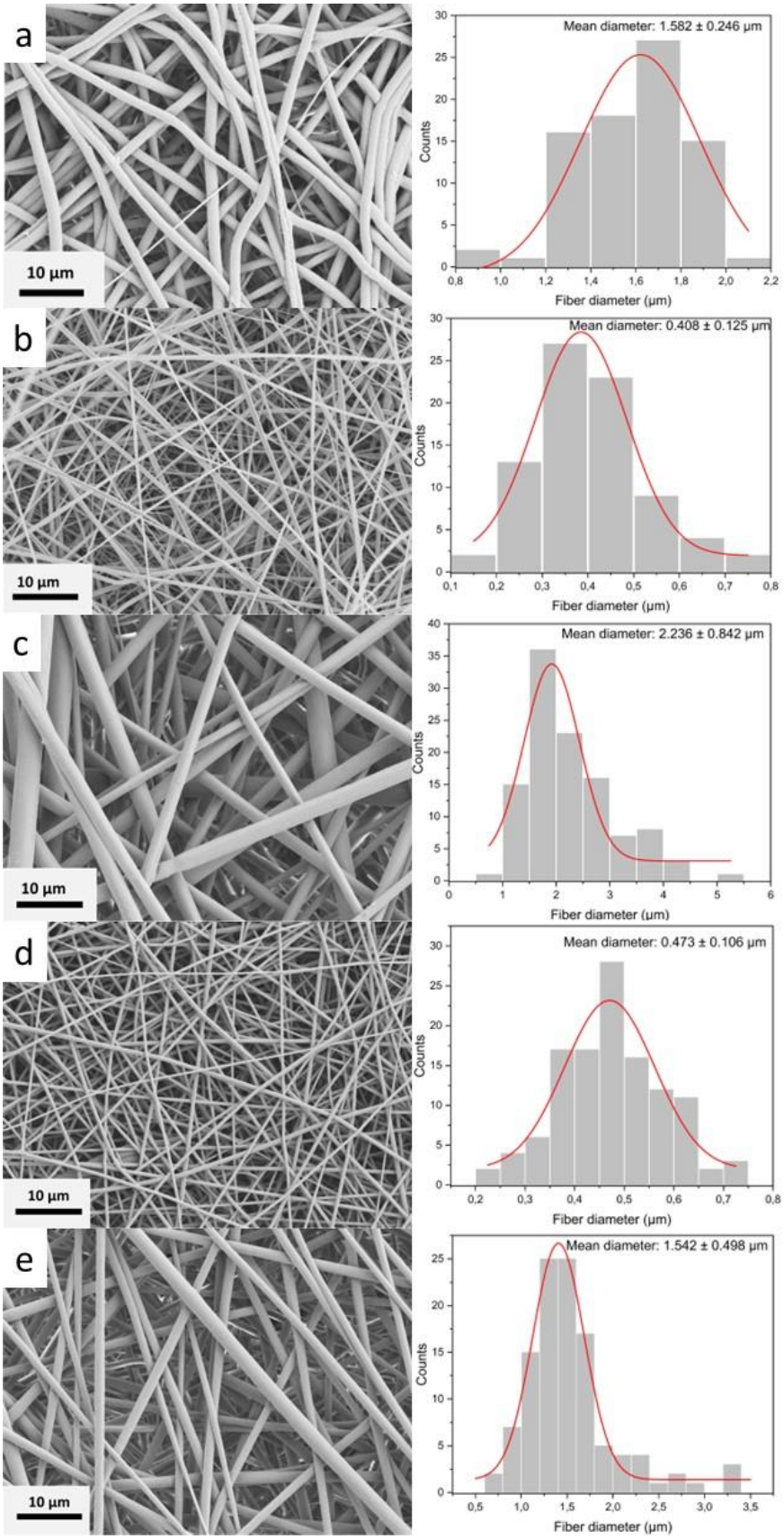

Figure 9 SEM images of nanofibers and their histograms showing the distributions of fiber diameters (a) PCL, (b) SF, (c) PS1, (d) PS2, and (e) PS2PS1.

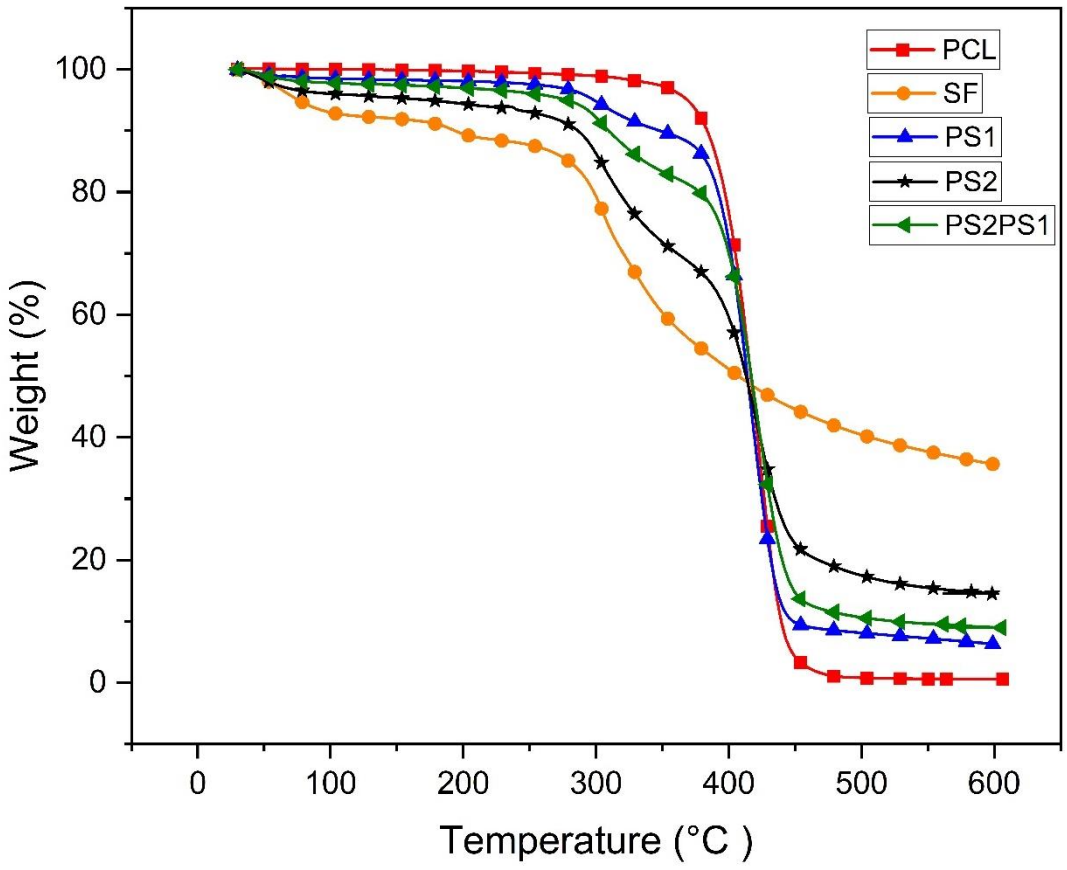

Figure 10 TGA analysis shows nanofibers' weight percentage change with increasing temperature.

Table 2 Overall weight loss nanofibers in TGA.

Polymer nanofibers	**Overall weight loss(%)**
PCL	99.41%
SF	64.33%
PS1	93.68%
PS2	85.53%
PS2PS1	91.02%

2.4.Mechanical Properties of polymer nanofibers

Samples are required to possess adequate mechanical strength to replace a skin structure in the body [64]. Figure 11 gives the stress vs. strain curves of each nanofiber in comparison. Pure SF had a Young's modulus of 64.9 MPa which means that it can resist the most load before failing among the samples. SF possessed a maximum tensile stress of 1700 KPa, whereas it failed suddenly at the tensile strain of 8%. This sudden failure could be caused by the stiffening effect caused by the CN groups in the structure. On the other hand, PCL possessed Young's modulus of 10.1 MPa.

It was observed that the addition of SF into PCL up to some extent increased Young's modulus to 50.4 MPa in the PS1 sample and maximum tensile stress improved to 2800 KPa. It indicates that when a specific amount of SF is added to PCL in the blend, it improves the nanofiber's mechanical strength. This could be resulted from the physical interactions between the PCL and SF fibers due to the thinner SF-nanofiber membrane formation within the thicker PCL fibers [65].

It is believed that addition of SF into PCL improves Young's modulus, since SF increased the stiffness and the structural integrity of the scaffolds [66]. Interestingly, PS2 obtained a lower Young's modulus, 36.1 MPa, and tensile stress compared to PS1. It indicates that increasing SF content in the blend after a specific amount does not contribute to the mechanical strength of the fibers as much.

In a similar study performed by Fadaie et al., the addition of chitosan into PCL improved Young's modulus of the electrospun 5.4 times, from 6.06 ± 1.4 MPa to 32.9 ± 4.4 MPa. The reason for this mechanical improvement was attributed to the intermolecular interactions between PCL molecular chains and chitosan nanofibrils which also possesses C-N groups in its structure just like SF [67].

PS2PS1 had Young's modulus and the maximum tensile stress of 59.8 MPa and 2450 KPa, respectively. Overall, it can be concluded that the PS2PS1 sample showed the best mechanical performance in combination with both Young's modulus and the maximum tensile stress. Table 3 shows the mechanical properties of the scaffolds.

Mechanical properties of skin are widely examined in the literature and the results of the studies vary depending on the age, sex, sample type, and the region the tissue excised.

Meijer et al. examined the mechanical property of human forearm skin and found Young's modulus as 25 MPa, similar to Young's modulus of PS2, under a uniaxial tensile test [68]. In another study, Annaidh et al. found Young's modulus of back skin tissue of people, at the age of 81-97 years, as 83.33 ± 4.9 MPa [69]. Gallagher et al. obtained Young's modulus of back as between 48.4-118.2 MPa [70]. In addition, Ankerson et al. stated Young's modulus of abdomen skin to be 14.96 MPa [71].

Additionally, Figure 12-16 gives mechanical testing images of polymer nanofibers. Figures showed that all samples other than SF experienced high elongation until the break. However, SF experienced a sudden failure at around 50 sec.

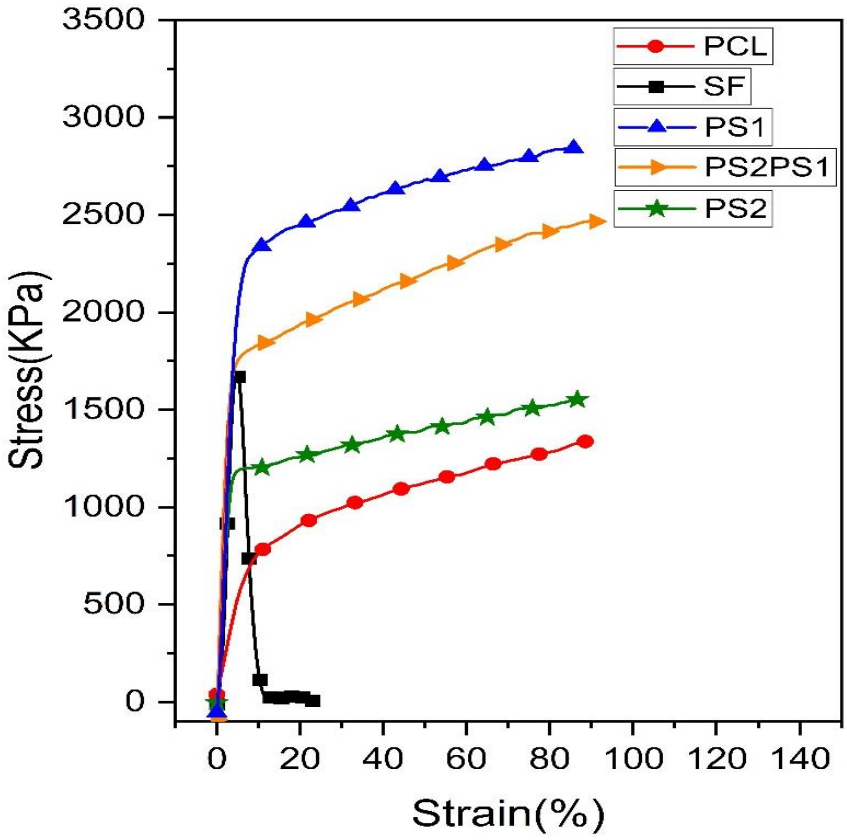

Figure 11 Stress vs. strain curve of nanofibers.

Table 3 Mechanical properties of polymer nanofibers.

Polymer nanofibers	**Young's modulus (MPa)**	**Maximum stress (KPa)**	**Maximum strain (%)**
PCL	10.1	1300	88
SF	64.9	1700	8
PS1	50.4	2800	85
PS2	36.1	1500	86
PS2PS1	59.8	2450	90

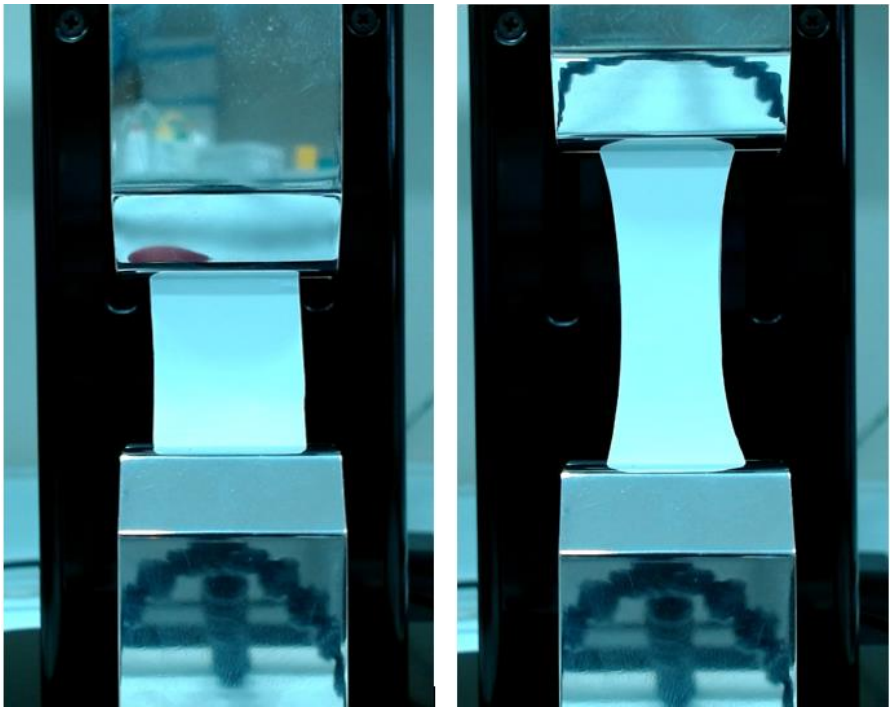

Figure 12 Mechanical test images of PCL after 1 sec and 50 sec.

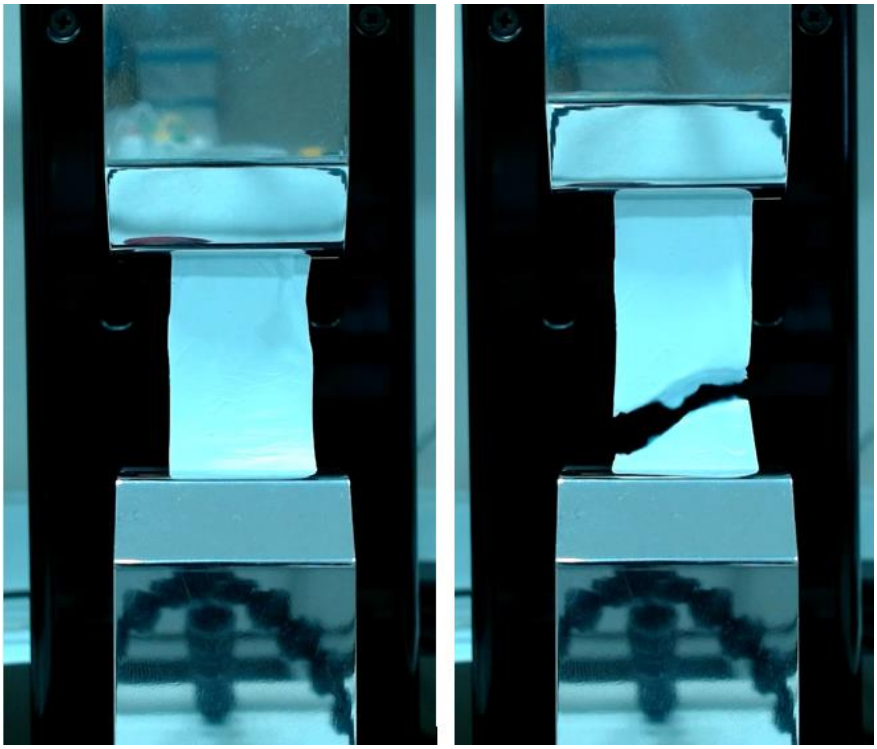

Figure 13 Mechanical test images of SF after 1 sec and 50 sec.

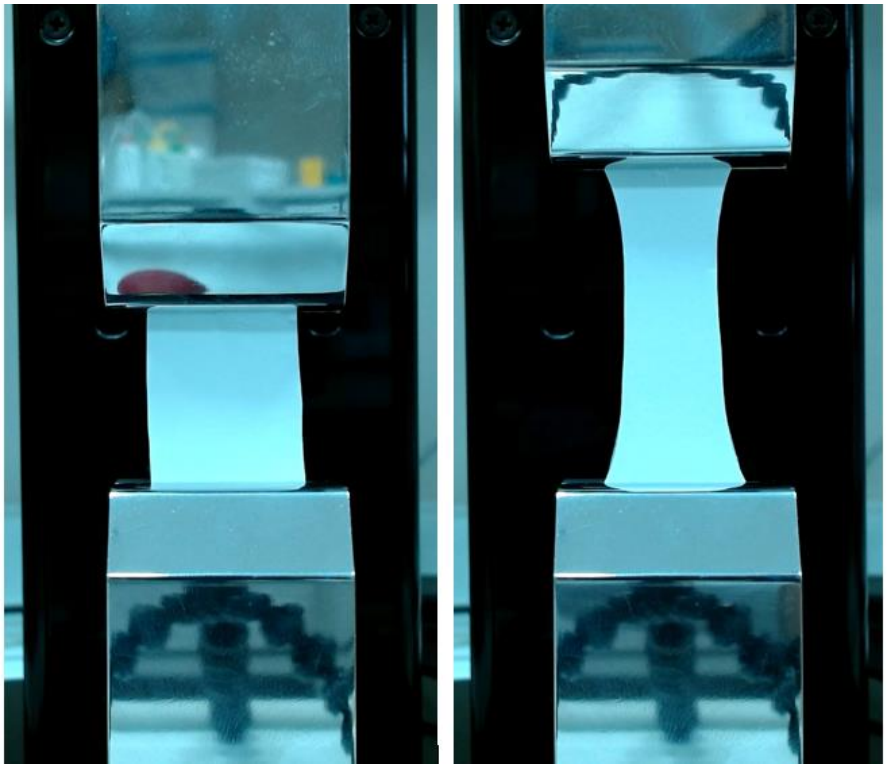

Figure 14 Mechanical test images of PS1 after 1 sec and 50 sec.

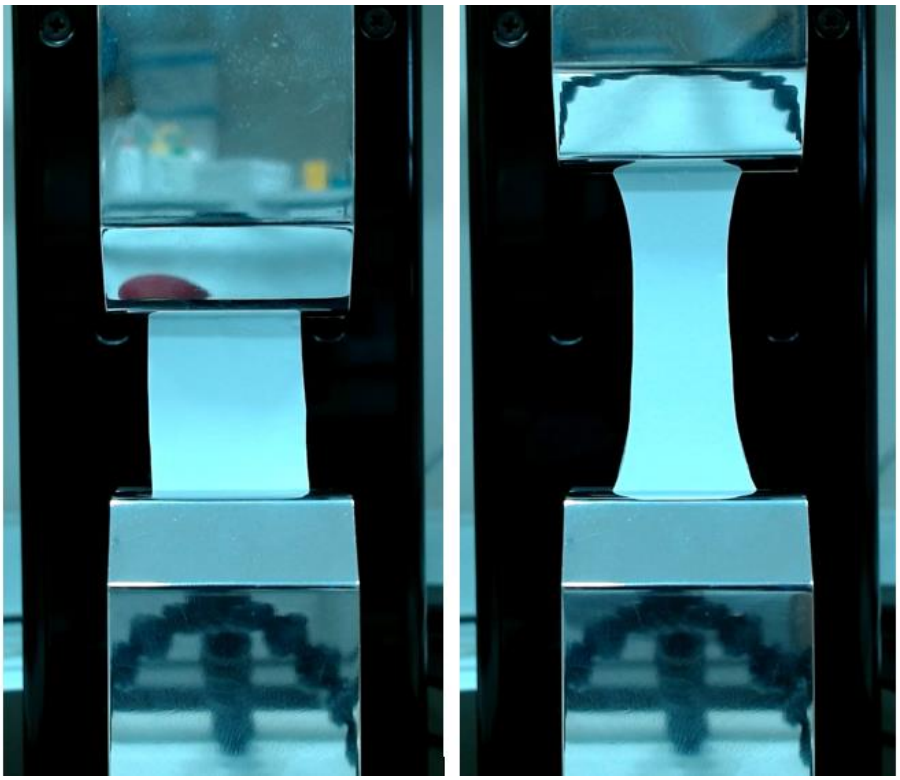

Figure 15 Mechanical test images of PS2 after 1 sec and 50 sec.

Figure 16 Mechanical test images of PS2PS1 after 1 sec and 50 sec.

2.5.Contact Angle Measurements

Hydrophobicity/hydrophilicity is a significant factor for tissue engineering products which influences cell adhesion and consequently the cell distribution on the materials. Hydrophilic surfaces are more favorable for cells to attach and proliferate on the substrate. On the opposite, hydrophobic surfaces have poor cell attachment capacity and do not support cell proliferation as hydrophilic surfaces do [72].

Hydrophilic materials allow more passage of biomolecules, nutrients, and wastes through nanofibers leading to enhanced cellular function. The water contact angle of a sample is measured by putting a drop of water on a sample and measuring the angle of the droplet about the sample level. Material is considered hydrophobic if the contact angle of the water drop is greater than 90° and it is hydrophilic if is less than 90° [73]. Figure 17 depicts the water contact angle of the six samples.

It was observed that the PCL was hydrophobic with a contact angle of 119.1 ± 2.53° (Figure 17a). On opposite, the SF sample had a contact angle of 37.9 ± 4.94 ° which makes it very hydrophilic (Figure 17b). SF is quite hydrophilic thanks to its functional hydrophilic amide (-CONH) and hydroxyl (-OH) groups [62]. PS1 and PS2 had contact angles of 36.7 ± 6.17 ° (Figure 17c) and 33.7 ± 1.53° (Figure 17d), respectively. It was expected since the PCL content of PS1 is greater than PS2 which makes it more hydrophobic. In theory, it was expected that the SF would have a smaller contact angle compared to PS1 and PS2. However, the results show that SF had a greater contact angle than PS1 and PS2. This could result from the surface roughness of the samples. Surface roughness also has an impact on the hydrophilicity and with an increase in roughness, the hydrophilicity increases as well [74]. So, it could be concluded that the surface roughnesses of PS1 and PS2 are more than the surface roughness of the SF resulted from fiber distribution.

The contact angle of PS2PS1 shows the second layer of the nanofibers. The contact angle of PS1PS2 comes from PCL: SF (3:7) composition and PS2PS1 comes from PCL: SF (7:3) composition. The contact angle of PS2PS1 was 44.3 ± 0.44° (Figure 17e). Overall, all samples show suitable hydrophilicity to be used as a scaffold other than PCL.

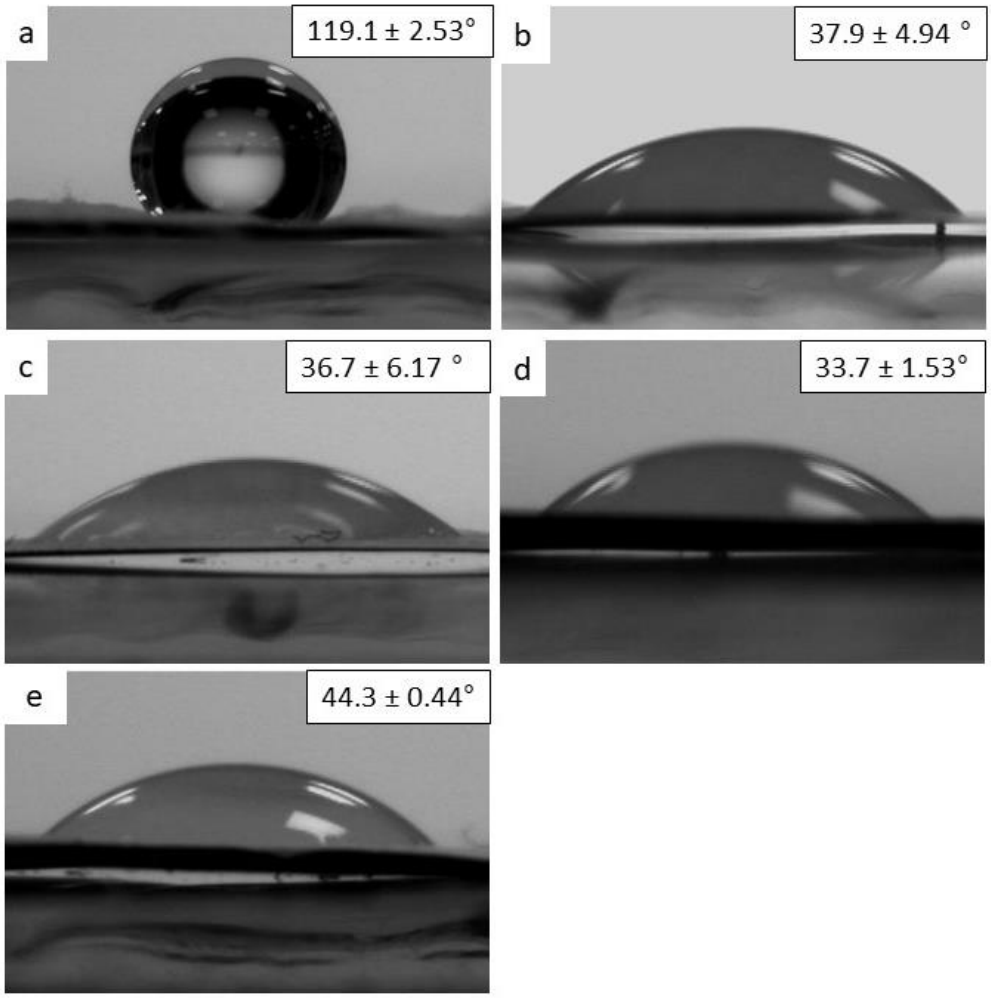

Figure 17 Contact angle of nanofibers (a) PCL, (b) SF, (c) PS1, (d) PS2, and (e) PS2PS1.

2.6.Pore Size and Surface Analysis of polymer nanofibers

Pore size has an important effect on cell migration and proliferation. When the pore size is too small, cells would not be able to migrate through the scaffold which will restrict the nutrient diffusion and waste removal from the scaffold. On the opposite, if the pore size is too large the surface area will decrease and there will not be enough space for cells to attach to the scaffold [75]. The pore size analysis of the scaffolds was performed with BET analysis and the results are given in Table 4. All nanofibers had similar pore sizes of around 17.3 Å.

The surface area of samples was evaluated using the Multi-point surface area and BJH surface area methods. From BJH analysis, the greatest surface area was PS2's with 13.929 m^2/g, and the smallest surface area was PCL's with 1.688 m^2/g. From Multi-point surface area analysis, the greatest and the smallest surface areas belonged to PS2 with 15.637 m^2/g and PCLs with 2.435 m^2/g, respectively. Overall, it could be concluded that the addition of SF into PCL increases the surface area of the scaffolds.

Chen et al. stated in one of their studies that fibers obtaining more uniform and smaller diameters produce higher surface area-to-volume ratios. [69]. In our study, PS2 possessed one of the lowest mean fiber diameters and the most uniform fiber diameter distributions among the samples. This could the reason that PS2 possessed the highest surface area among the samples. Can-Herrera et al. analyzed the impact of different voltages on fiber surface area and diameter. They found that PCL obtained higher surface area as voltage decreased due to the thinner fiber formation [76].

PS2PS1 had a surface area of 7.190 m^2/g which is a value in between the surface area of PS1 and PS2, as it was made up of these polymer blends layer by layer. According to pore volume analysis, PS2 gave the greatest pore volume of 0.029 cc/g and PCL gave the smallest pore volume of 0.004 cc/g.

Table 4 BET analysis of nanofibers.

Polymer nanofiber	BJH surface area	Pore volume	Pore diameter	Multi-point surface area
PCL	1.688 m^2/g	0.004 cc/g	17.310 Å	2.435 m^2/g
SF	6.322 m^2/g	0.015 cc/g	17.333 Å	7.115 m^2/g
PS1	3.665 m^2/g	0.007 cc/g	17.319 Å	3.619 m^2/g
PS2	13.929 m^2/g	0.029 cc/g	17.315 Å	15.637 m^2/g
PS2PS1	7.190 m^2/g	0.015 cc/g	17.292 Å	2.917 m^2/g

2.7. In vitro biodegradation analysis

Biodegradability is one of the most important properties of a scaffold which also has an impact on the mechanical features. Scaffolds should possess an adequate rate of biodegradability to allow the existing tissue to replace the scaffold by regeneration [77]. Table 5 gives the degradation percentage of the samples after 12 h and 24 h. Proteinase K enzyme allows the breakdown of SF polymer chains into peptides and even into amino acids [78]. PCL degradation by the Proteinase K enzyme occurs via the surface erosion of the samples [79]. Figure 18 illustrates the degradation profiles of the scaffolds.

PCL did not experience a high level of weight loss where the degradation percentage was 7.5 % and 14.8 % after 12 h and 24 h, respectively. Similarly, PS1 which has the highest PCL content in its blend showed only a moderately higher degradation rate than PCL with 12.9 % and 20.17 % after 12 h and 24 h, respectively. SF started to lose its integrity after around 5-6 h and showed no remaining fiber with 100 % degradation after 12 h. This fast degradation effect of Proteinase K on SF is correlated with the previous studies as it was stated that the enzyme highly attacks peptide bonds. As Proteinase K attacks these bonds large protein fragments are digested into smaller pieces and the β-sheet structures are broken into α-helices and random coils [80].

PS2 showed the second highest degradation percentage after SF as it contains the highest SF amount among the blend scaffolds with 51 % and 23.18 % after 12 h and 24 h,

respectively. PS2PS1 had the degradation percentages between PS1 and PS1 as they are the half-mix of PS1 and PS2. The degradation percentage of PS2PS1 was 18.17 % and 23.18 % after 12 h and 24 h, respectively. The degradation percentage of PS2PS1 was 31.6 % and 46.17 % after 12 h and 24 h, respectively. Overall, the degradation percentage increased with the increasing amount of SF in the scaffold structure.

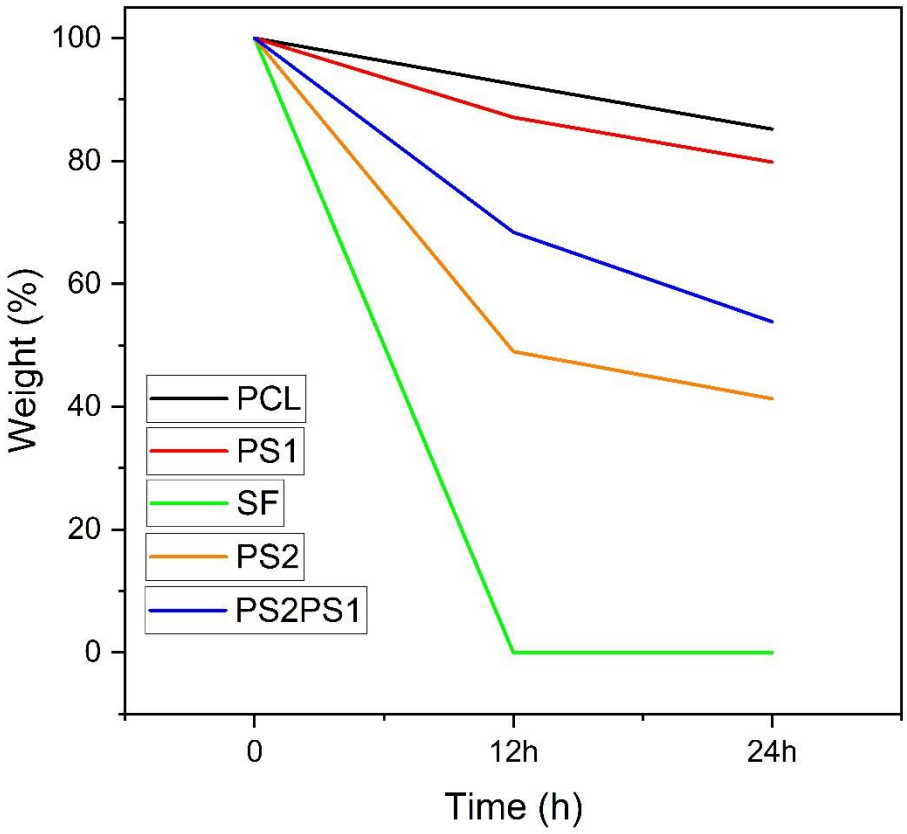

Figure 18 Degradation profiles of polymer nanofibers after 12 h and 24h.

Table 5 In vitro biodegradation percentages of nanofibers after 12 h and 24 h.

Polymer nanofiber	**Degradation percentage**	
	12 h (%)	24 h (%)
PCL	7.50 ± 6.12	14.8 ± 8.74
SF	100.00 ± 0.00	100.00 ± 0.00
PS1	12.93 ± 5.07	20.17 ± 0.24
PS2	51.09 ± 7.28	58.70 ± 6.35
PS2PS1	31.67 ± 1.36	46.17 ± 2.12

2.8. Cell Proliferation and Viability

The proliferation and viability rate of primary human epidermal keratinocyte cells (40 000 cells/nanofiber) on the PCL, SF, PS2PS1 nanofibers were assessed using calcein-AM and EthD-1 staining (Figure 19). After 2 days, the viability of the cells improved and low cell death was observed, indicating the cytocompatibility of all scaffolds. It was examined that cells adhered to the fibers. At the end of the 7 days, cells kept their viability on all scaffolds, and only a few dead cells were observed.

Figure 20 shows the XTT proliferation results of the primary human epidermal keratinocyte cells (40 000 cells/nanofiber) on nanofibers. It is observed that cells maintained their functions on nanofibers and showed improved proliferation from day 2 to 7. PS2PS1 showed the highest proliferation compared to others. The reason could be that since it contains both PS1 and PS2 layer by layer, the advanced properties of each layer contributed to the cell functionality. PS1 supplied the structural strength and PS2 provided the required bioactivity, coming from SF, to the final scaffold. Overall, it could be resulted that blending PCL with SF provided a better environment for cell proliferation and viability.

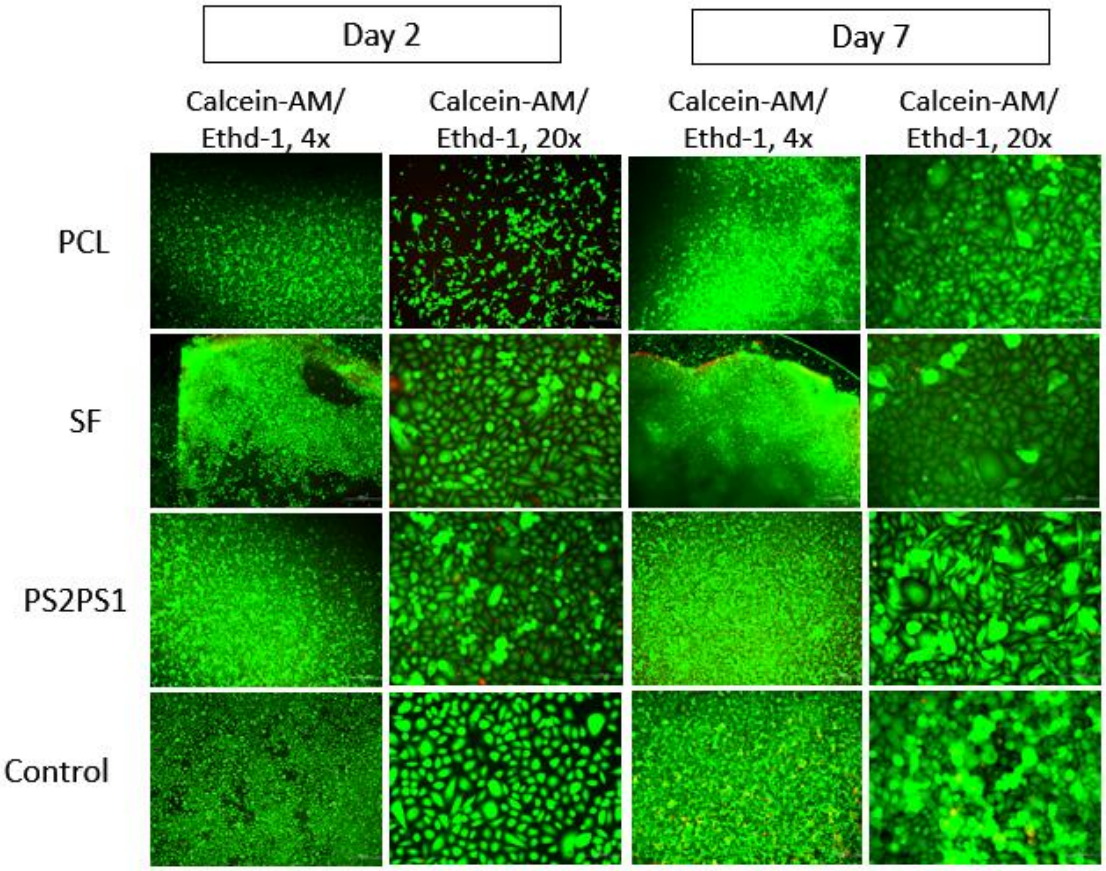

Figure 19 Cell Viability Test of primary human epidermal keratinocyte cells on nanofibers.

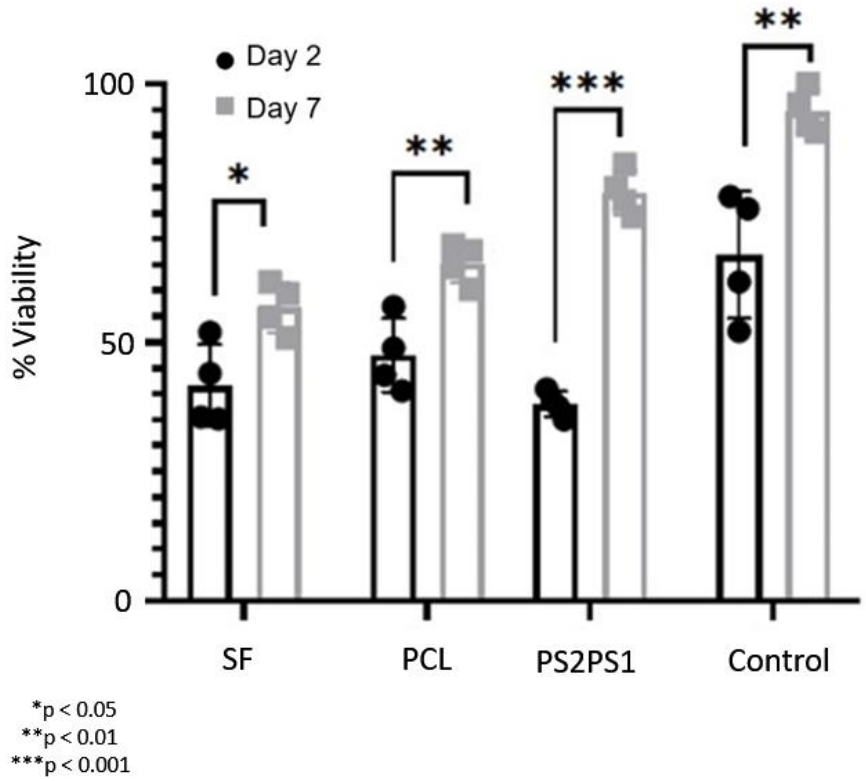

Figure 20 Cell Proliferation (XTT) assay of nanofibers.

3. CONCLUSION

In this study, various PCL/SF-based nanofibers were fabricated, and their characteristics were examined such as morphology, mechanical strength, hydrophilicity, surface area, pore size, in vitro degradation, and proliferation capacities. According to SEM analysis, all samples showed homogenous fiber distribution without beads. SF had better thermal stability compared to PCL and with increasing PCL content thermal weight loss of the nanofibers increased. The tensile strength of PCL improved with the incorporation of SF as it provided intermolecular interactions within the nanofibers. In addition, Young's modulus of the samples also was enhanced with the addition of SF due to the increase in stiffness and the structural integrity of the samples. The hydrophilicity of five samples was sufficient, with contact angles of between 33-48°, apart from PCL. Lastly, seeded keratinocytes showed the best proliferation and viability in the PS2PS1 sample after 7 days.

References

[1] M. A. Maranduca *et al.*, "Synthesis and physiological implications of melanic pigments (review)," *Oncol. Lett.*, vol. 17, no. 5, pp. 4183–4187, 2019, doi: 10.3892/ol.2019.10071.

[2] B. Ramy Abdlaty and Me. BEng, "Hyperspectral Imaging and Data Analysis of Skin Erythema Post Radiation Therapy Treatment," no. September 2016, 2016.

[3] T. Someya and M. Amagai, "Toward a new generation of smart skins," *Nat. Biotechnol.*, vol. 37, no. 4, pp. 382–388, 2019, doi: 10.1038/s41587-019-0079-1.

[4] K. Raziyeva, Y. Kim, Z. Zharkinbekov, K. Kassymbek, S. Jimi, and A. Saparov, "Immunology of acute and chronic wound healing," *Biomolecules*, vol. 11, no. 5, pp. 1–25, 2021, doi: 10.3390/biom11050700.

[5] M. M. Demir, I. Yilgor, E. Yilgor, and B. Erman, "Electrospinning of polyurethane fibers," *Polymer (Guildf).*, vol. 43, no. 11, pp. 3303–3309, 2002, doi: 10.1016/S0032-3861(02)00136-2.

[6] Y. Z. Long, X. Yan, X. X. Wang, J. Zhang, and M. Yu, *Electrospinning*. Elsevier Inc., 2018. doi: 10.1016/B978-0-323-51270-1.00002-9.

[7] J. Hong, M. Yeo, G. H. Yang, and G. Kim, "Cell-electrospinning and its application for tissue engineering," *Int. J. Mol. Sci.*, vol. 20, no. 24, 2019, doi: 10.3390/ijms20246208.

[8] M. Ziabari, V. Mottaghitalab, and A. K. Haghi, "Application of direct tracking method for measuring electrospun nanofiber diameter," *Brazilian J. Chem. Eng.*, vol. 26, no. 1, pp. 53–62, 2009, doi: 10.1590/S0104-66322009000100006.

[9] H. L. Schreuder-Gibson and P. Gibson, "Applications of electrospun nanofibers in current and future materials," *ACS Symp. Ser.*, vol. 918, no. January, pp. 121–136, 2006, doi: 10.1021/bk-2006-0918.ch009.

[10] I. S. Chronakis, "Novel nanocomposites and nanoceramics based on polymer nanofibers using electrospinning process - A review," *J. Mater. Process. Technol.*, vol. 167, no. 2–3, pp. 283–293, 2005, doi:

10.1016/j.jmatprotec.2005.06.053.

[11] T. H. Barker, “The role of ECM proteins and protein fragments in guiding cell behavior in regenerative medicine,” *Biomaterials*, vol. 32, no. 18, pp. 4211–4214, 2011, doi: 10.1016/j.biomaterials.2011.02.027.

[12] D. I. Braghirolli, D. Steffens, and P. Pranke, “Electrospinning for regenerative medicine: A review of the main topics,” *Drug Discov. Today*, vol. 19, no. 6, pp. 743–753, 2014, doi: 10.1016/j.drudis.2014.03.024.

[13] R. A. Stanton and D. A. Billmire, “Skin resurfacing for the burned patient,” *Clin. Plast. Surg.*, vol. 29, no. 1, pp. 29–51, 2002, doi: 10.1016/S0094-1298(03)00085-3.

[14] A. Andreassi, R. Bilenchi, M. Biagioli, and C. D’Aniello, “Classification and pathophysiology of skin grafts,” *Clin. Dermatol.*, vol. 23, no. 4, pp. 332–337, 2005, doi: 10.1016/j.clindermatol.2004.07.024.

[15] R. A. F. Clark, K. Ghosh, and M. G. Tonnesen, “Tissue engineering for cutaneous wounds,” *J. Invest. Dermatol.*, vol. 127, no. 5, pp. 1018–1029, 2007, doi: 10.1038/sj.jid.5700715.

[16] J. williams, B, “乳鼠心肌提取 HHS Public Access,” *Physiol. Behav.*, vol. 176, no. 3, pp. 139–148, 2019, doi: 10.1016/j.burns.2018.02.029.SKIN.

[17] A. V. Nasalapure, R. K. Chalannavar, R. S. Gani, R. B. Malabadi, and D. R. Kasai, “Tissue engineering of skin: A review,” *Trends Biomater. Artif. Organs*, vol. 31, no. 2, pp. 69–80, 2017.

[18] Z. Li *et al.*, “Injectable gelatin derivative hydrogels with sustained vascular endothelial growth factor release for induced angiogenesis,” *Acta Biomater.*, vol. 13, pp. 88–100, 2015, doi: 10.1016/j.actbio.2014.11.002.

[19] J. Qin, F. Chen, P. Wu, and G. Sun, “Recent Advances in Bioengineered Scaffolds for Cutaneous Wound Healing,” *Front. Bioeng. Biotechnol.*, vol. 10, no. March, pp. 1–18, 2022, doi: 10.3389/fbioe.2022.841583.

[20] I. Negut, G. Dorcioman, and V. Grumezescu, “Sca ff olds for Wound Healing Applications,” 2020.

[21] Y. Wang *et al.*, "A self-adapting hydrogel based on chitosan/oxidized konjac glucomannan/AgNPs for repairing irregular wounds," *Biomater. Sci.*, vol. 8, no. 7, pp. 1910–1922, 2020, doi: 10.1039/c9bm01635j.

[22] Y. Liang, Z. Li, Y. Huang, R. Yu, and B. Guo, "Dual-Dynamic-Bond Cross-Linked Antibacterial Adhesive Hydrogel Sealants with On-Demand Removability for Post-Wound-Closure and Infected Wound Healing," *ACS Nano*, vol. 15, no. 4, pp. 7078–7093, 2021, doi: 10.1021/acsnano.1c00204.

[23] X. Zhang, G. Chen, Y. Liu, L. Sun, L. Sun, and Y. Zhao, "Black Phosphorus-Loaded Separable Microneedles as Responsive Oxygen Delivery Carriers for Wound Healing," *ACS Nano*, vol. 14, no. 5, pp. 5901–5908, 2020, doi: 10.1021/acsnano.0c01059.

[24] L. Gao *et al.*, "A multifunctional shape-adaptive and biodegradable hydrogel with hemorrhage control and broad-spectrum antimicrobial activity for wound healing," *Biomater. Sci.*, vol. 8, no. 24, pp. 6930–6945, 2020, doi: 10.1039/d0bm00800a.

[25] J. Hu *et al.*, "Clinical efficacy of wet dressing combined with chitosan wound dressing in the treatment of deep second-degree burn wounds: A prospective, randomised, single-blind, positive control clinical trial," *Int. Wound J.*, vol. 20, no. 3, pp. 699–705, 2023, doi: 10.1111/iwj.13911.

[26] Y. Dong, S. Liao, M. Ngiam, C. K. Chan, and S. Ramakrishna, "Degradation behaviors of electrospun resorbable polyester nanofibers," *Tissue Eng. - Part B Rev.*, vol. 15, no. 3, pp. 333–351, 2009, doi: 10.1089/ten.teb.2008.0619.

[27] P. Dinarvand *et al.*, "Function of poly (lactic-co-glycolic acid) nanofiber in reduction of adhesion bands," *J. Surg. Res.*, vol. 172, no. 1, pp. e1–e9, 2012, doi: 10.1016/j.jss.2011.10.014.

[28] A. Mohebali, M. Abdouss, and F. Afshar Taromi, "Fabrication of biocompatible antibacterial nanowafers based on HNT/PVA nanocomposites loaded with minocycline for burn wound dressing," *Mater. Sci. Eng. C*, vol. 110, no. December 2019, p. 110685, 2020, doi: 10.1016/j.msec.2020.110685.

[29] M. Zehra *et al.*, "Oxygen generating polymeric nano fibers that stimulate angiogenesis and show efficient wound healing in a diabetic wound model," *Int.*

J. Nanomedicine, vol. 15, pp. 3511–3522, 2020, doi: 10.2147/IJN.S248911.

[30] G. S. Liu *et al.*, "In Situ Electrospinning Iodine-Based Fibrous Meshes for Antibacterial Wound Dressing," *Nanoscale Res. Lett.*, vol. 13, 2018, doi: 10.1186/s11671-018-2733-9.

[31] M. Sheikholeslam, M. E. E. Wright, M. G. Jeschke, and S. Amini-Nik, "Biomaterials for Skin Substitutes," *Adv. Healthc. Mater.*, vol. 7, no. 5, pp. 1–20, 2018, doi: 10.1002/adhm.201700897.

[32] C. Viezzer, R. Mazzuca, D. C. Machado, M. M. de Camargo Forte, and J. L. Gómez Ribelles, "A new waterborne chitosan-based polyurethane hydrogel as a vehicle to transplant bone marrow mesenchymal cells improved wound healing of ulcers in a diabetic rat model," *Carbohydr. Polym.*, vol. 231, no. December 2019, p. 115734, 2020, doi: 10.1016/j.carbpol.2019.115734.

[33] A. R. Abbasi *et al.*, "Bioinspired sodium alginate based thermosensitive hydrogel membranes for accelerated wound healing," *Int. J. Biol. Macromol.*, vol. 155, pp. 751–765, 2020, doi: 10.1016/j.ijbiomac.2020.03.248.

[34] O. Gsib, L. J. Eggermont, C. Egles, and S. A. Bencherif, "Engineering a macroporous fibrin-based sequential interpenetrating polymer network for dermal tissue engineering," *Biomater. Sci.*, vol. 8, no. 24, pp. 7106–7116, 2020, doi: 10.1039/d0bm01161d.

[35] R. Song, M. Murphy, C. Li, K. Ting, C. Soo, and Z. Zheng, "Current development of biodegradable polymeric materials for biomedical applications," *Drug Des. Devel. Ther.*, vol. 12, pp. 3117–3145, 2018, doi: 10.2147/DDDT.S165440.

[36] R. Dwivedi *et al.*, "Polycaprolactone as biomaterial for bone scaffolds: Review of literature," *J. Oral Biol. Craniofacial Res.*, vol. 10, no. 1, pp. 381–388, 2020, doi: 10.1016/j.jobcr.2019.10.003.

[37] H. M. Powell and S. T. Boyce, "Engineered human skin fabricated using electrospun collagen-PCL blends: Morphogenesis and mechanical properties," *Tissue Eng. - Part A*, vol. 15, no. 8, pp. 2177–2187, 2009, doi: 10.1089/ten.tea.2008.0473.

[38] E. R. Ghomi *et al.*, “Electrospun Aligned PCL/Gelatin Scaffolds Mimicking the Skin ECM for Effective Antimicrobial Wound Dressings,” *Adv. Fiber Mater.*, vol. 5, no. 1, pp. 235–251, 2023, doi: 10.1007/s42765-022-00216-w.

[39] S. Metwally, D. P. Ura, Z. J. Krysiak, Ł. Kaniuk, P. K. Szewczyk, and U. Stachewicz, “Electrospun PCL patches with controlled fiber morphology and mechanical performance for skin moisturization via long-term release of hemp oil for atopic dermatitis,” *Membranes (Basel).*, vol. 11, no. 1, pp. 1–13, 2021, doi: 10.3390/membranes11010026.

[40] G. Shen, X. Hu, G. Guan, and L. Wang, “Surface modification and characterisation of silk fibroin fabric produced by the layer-by-layer self-assembly of multilayer alginate/regenerated silk fibroin,” *PLoS One*, vol. 10, no. 4, 2015, doi: 10.1371/journal.pone.0124811.

[41] W. Sun, D. A. Gregory, M. A. Tomeh, and X. Zhao, “Silk fibroin as a functional biomaterial for tissue engineering,” *Int. J. Mol. Sci.*, vol. 22, no. 3, pp. 1–28, 2021, doi: 10.3390/ijms22031499.

[42] H. W. Ju *et al.*, “Wound healing effect of electrospun silk fibroin nanomatrix in burn-model,” *Int. J. Biol. Macromol.*, vol. 85, pp. 29–39, 2016, doi: 10.1016/j.ijbiomac.2015.12.055.

[43] Ł. Mazurek, M. Szudzik, M. Rybka, and M. Konop, “Silk Fibroin Biomaterials and Their Beneficial Role in Skin Wound Healing,” *Biomolecules*, vol. 12, no. 12, 2022, doi: 10.3390/biom12121852.

[44] P. Guo *et al.*, “Regulating the mechanics of silk fibroin scaffolds promotes wound vascularization,” *Biochem. Biophys. Res. Commun.*, vol. 574, pp. 78–84, 2021, doi: 10.1016/j.bbrc.2021.08.026.

[45] S. He *et al.*, “Heparinized silk fibroin hydrogels loading FGF1 promote the wound healing in rats with full-thickness skin excision,” *Biomed. Eng. Online*, vol. 18, no. 1, pp. 1–12, 2019, doi: 10.1186/s12938-019-0716-4.

[46] P. Yang *et al.*, “Insulin-Containing Wound Dressing Promotes Diabetic Wound Healing Through Stabilizing HIF-1α,” *Front. Bioeng. Biotechnol.*, vol. 8, no. December, pp. 1–10, 2020, doi: 10.3389/fbioe.2020.592833.

[47] D. N. Rockwood, R. C. Preda, T. Yücel, X. Wang, M. L. Lovett, and D. L. Kaplan, “Materials fabrication from Bombyx mori silk fibroin,” *Nat. Protoc.*, vol. 6, no. 10, pp. 1612–1631, 2011, doi: 10.1038/nprot.2011.379.

[48] K. Izumi, H. Terashi, C. L. Marcelo, and S. E. Feinberg, “Development and characterization of a tissue-engineered human oral mucosa equivalent produced in a serum-free culture system,” *J. Dent. Res.*, vol. 79, no. 3, pp. 798–805, 2000, doi: 10.1177/00220345000790030301.

[49] G. R. Bayar, S. Kuo, C. L. Marcelo, and S. E. Feinberg, “In Vitro Development of a Mucocutaneous Junction for Lip Reconstruction,” *J. Oral Maxillofac. Surg.*, vol. 74, no. 11, pp. 2317–2326, 2016, doi: 10.1016/j.joms.2016.04.002.

[50] Y.-Q. Zhang, “SDS-PAGE for Silk Fibroin Protein,” *Bio-Protocol*, vol. 8, no. 20, 2018, doi: 10.21769/bioprotoc.3054.

[51] E. Kamalha, Y. Zheng, Y. Zeng, and M. N. Fredrick, “FTIR and WAXD study of regenerated silk fibroin,” *Advanced Materials Research*, vol. 677. pp. 211–215, 2013. doi: 10.4028/www.scientific.net/AMR.677.211.

[52] M. Wöltje, A. Kölbel, D. Aibibu, and C. Cherif, “A fast and reliable process to fabricate regenerated silk fibroin solution from degummed silk in 4 hours,” *Int. J. Mol. Sci.*, vol. 22, no. 19, 2021, doi: 10.3390/ijms221910565.

[53] A. L. Marquez, I. E. Gareis, F. J. Dias, C. Gerhard, and M. F. Lezcano, “Methods to Characterize Electrospun Scaffold Morphology: A Critical Review,” *Polymers (Basel).*, vol. 14, no. 3, pp. 1–22, 2022, doi: 10.3390/polym14030467.

[54] S. Sridhar, J. R. Venugopal, R. Sridhar, and S. Ramakrishna, “Cardiogenic differentiation of mesenchymal stem cells with gold nanoparticle loaded functionalized nanofibers,” *Colloids Surfaces B Biointerfaces*, vol. 134, pp. 346–354, 2015, doi: 10.1016/j.colsurfb.2015.07.019.

[55] J. Lv, L. Chen, Y. Zhu, L. Hou, and Y. Liu, “Promoting epithelium regeneration for esophageal tissue engineering through basement membrane reconstitution,” *ACS Appl. Mater. Interfaces*, vol. 6, no. 7, pp. 4954–4964, 2014, doi: 10.1021/am4059809.

[56] A. H. P. Chan *et al.*, “Altered processing enhances the efficacy of small-diameter

silk fibroin vascular grafts," *Sci. Rep.*, vol. 9, no. 1, pp. 1–14, 2019, doi: 10.1038/s41598-019-53972-y.

[57] P. Karuppuswamy, J. R. Venugopal, B. Navaneethan, A. L. Laiva, S. Sridhar, and S. Ramakrishna, "Functionalized hybrid nanofibers to mimic native ECM for tissue engineering applications," *Appl. Surf. Sci.*, vol. 322, pp. 162–168, 2014, doi: 10.1016/j.apsusc.2014.10.074.

[58] M. M. n, Eunsung Mouradian, "基因的改变NIH Public Access," *Bone*, vol. 23, no. 1, pp. 1–7, 2008, doi: 10.1038/nature08365.Reconstructing.

[59] C. Gandhimathi, Y. J. Quek, H. Ezhilarasu, S. Ramakrishna, B. H. Bay, and D. K. Srinivasan, "Osteogenic differentiation of mesenchymal stem cells with silica-coated gold nanoparticles for bone tissue engineering," *Int. J. Mol. Sci.*, vol. 20, no. 20, pp. 1–15, 2019, doi: 10.3390/ijms20205135.

[60] Z. Luo, Y. Zhang, H. Zhou, J. Liao, X. Zhang, and Q. Wu, "A one-pot preparation of silk fibroin modified with polyurethane micro-particles," *New J. Chem.*, vol. 37, no. 10, pp. 3109–3115, 2013, doi: 10.1039/c3nj00501a.

[61] C. Du, J. Jin, Y. Li, X. Kong, K. Wei, and J. Yao, "Novel silk fibroin/hydroxyapatite composite films: Structure and properties," *Mater. Sci. Eng. C*, vol. 29, no. 1, pp. 62–68, 2009, doi: 10.1016/j.msec.2008.05.010.

[62] E. G. Bajsić *et al.*, "Preparation and characterization of electrospun pcl/silk fibroin scaffolds," *Chem. Biochem. Eng. Q.*, vol. 35, no. 1, pp. 31–42, 2021, doi: 10.15255/CABEQ.2020.1834.

[63] K. R. Fontenot *et al.*, "Application of a phosphazene derivative as a flam retardant for cotton fabric using conventional method and supercritical co2," *AATCC J. Res.*, vol. 1, no. 6, pp. 16–26, 2014, doi: 10.14504/ajr.1.6.3.

[64] C. Gandhimathi, Y. J. Quek, H. Ezhilarasu, S. Ramakrishna, B. H. Bay, and D. K. Srinivasan, "Osteogenic differentiation of mesenchymal stem cells with silica-coated gold nanoparticles for bone tissue engineering," *Int. J. Mol. Sci.*, vol. 20, no. 20, 2019, doi: 10.3390/ijms20205135.

[65] B. S. Kim, K. E. Park, M. H. Kim, H. K. You, J. Lee, and W. H. Park, "Effect of nanofiber content on bone regeneration of silk fibroin/poly(ε-caprolactone)

nano/microfibrous composite scaffolds," *Int. J. Nanomedicine*, vol. 10, no. January, pp. 485–502, 2015, doi: 10.2147/ijn.s72730.

[66] T. Roy *et al.*, "Core-shell nanofibrous scaffold based on polycaprolactone-silk fibroin emulsion electrospinning for tissue engineering applications," *Bioengineering*, vol. 5, no. 3, 2018, doi: 10.3390/bioengineering5030068.

[67] "S014486171830852X."

[68] R. Meijer, L. F. A. Douven, and C. W. J. Oomens, "Characterisation of anisotropic and non-linear behaviour of human skin in vivo," *Comput. Methods Biomech. Biomed. Engin.*, vol. 2, no. 1, pp. 13–27, 1999, doi: 10.1080/10255849908907975.

[69] A. Ní Annaidh, K. Bruyère, M. Destrade, M. D. Gilchrist, and M. Otténio, "Characterization of the anisotropic mechanical properties of excised human skin," *J. Mech. Behav. Biomed. Mater.*, vol. 5, no. 1, pp. 139–148, 2012, doi: 10.1016/j.jmbbm.2011.08.016.

[70] T. M. Express, "Downloaded 2023-01-18T09 : 19 : 28Z The UCD community has made this article openly available . Please share how this access benefits you . Your story matters ! (@ ucd _ oa) © Some rights reserved . For more information," 2014.

[71] K. A and L. A, "Mechanical Behaviour of Skin: A Review," *J. Mater. Sci. Eng.*, vol. 5, no. 4, 2016, doi: 10.4172/2169-0022.1000254.

[72] N. Al-Azzam and A. Alazzam, "Micropatterning of cells via adjusting surface wettability using plasma treatment and graphene oxide deposition," *PLoS One*, vol. 17, no. 6 June, pp. 1–14, 2022, doi: 10.1371/journal.pone.0269914.

[73] P. R. Elliott, S. P. Stagon, H. Huang, D. U. Furrer, S. F. Burlatsky, and T. P. Filburn, "Combined hydrophobicity and mechanical durability through surface nanoengineering," *Sci. Rep.*, vol. 5, pp. 1–5, 2015, doi: 10.1038/srep09260.

[74] C. Li, J. Zhang, J. Han, and B. Yao, "A numerical solution to the effects of surface roughness on water–coal contact angle," *Sci. Rep.*, vol. 11, no. 1, pp. 1–12, 2021, doi: 10.1038/s41598-020-80729-9.

[75] C. M. Murphy and F. J. O'Brien, "Understanding the effect of mean pore size on

cell activity in collagen-glycosaminoglycan scaffolds," *Cell Adhes. Migr.*, vol. 4, no. 3, pp. 377–381, 2010, doi: 10.4161/cam.4.3.11747.

[76] L. A. Can-Herrera, A. I. Oliva, M. A. A. Dzul-Cervantes, O. F. Pacheco-Salazar, and J. M. Cervantes-Uc, "Morphological and mechanical properties of electrospun polycaprolactone scaffolds: Effect of applied voltage," *Polymers (Basel).*, vol. 13, no. 4, pp. 1–16, 2021, doi: 10.3390/polym13040662.

[77] K. N. Bitar and E. Zakhem, "Biomedical Engineering and Computational Biology Design Strategies of Biodegradable Scaffolds for Tissue Regeneration," *Biomed. Eng. Comput. Biol.*, vol. 6, pp. 13–20, 2014, doi: 10.4137/BECB.S10961.RECEIVED.

[78] M. Rashighi and J. E. Harris, "乳鼠心肌提取 HHS Public Access," *Physiol. Behav.*, vol. 176, no. 3, pp. 139–148, 2017, doi: 10.1053/j.gastro.2016.08.014.CagY.

[79] "Macro Materials Eng - 2006 - Tsuji - Enzymatic Degradation of Biodegradable Polyester Composites of Poly L-lactic acid .pdf."

[80] A. Naidoo, K. Naidoo, N. Yende-zuma, and T. N. Gengiah, "Impact of silk biomaterial structure on proteolysis," *Acta Biomater.*, vol. 19, pp. 161–169, 2015, doi: 10.1016/j.actbio.2014.09.013.Impact.